

**REAL-TIME FEEDBACK CONTROL FOR
3D PRINTED ANTENNAS**

by

Collin Michael Wallish

A thesis submitted to the Faculty of the University of Delaware in partial fulfillment of the requirements for the degree of Master of Science in Electrical and Computer Engineering

Summer 2019

© 2019 Collin Michael Wallish
All Rights Reserved

**REAL-TIME FEEDBACK CONTROL FOR
3D PRINTED ANTENNAS**

by

Collin Michael Wallish

Approved: _____
Mark S. Mirotznik, Ph.D.
Professor in charge of thesis on behalf of the Advisory Committee

Approved: _____
Kenneth E. Barner, Ph.D.
Chair of the Department of Electrical and Computer Engineering

Approved: _____
Levi T. Thompson, Ph.D.
Dean of the College of Engineering

Approved: _____
Douglas J. Doren, Ph.D.
Interim Vice Provost for Graduate & Professional Education and Dean of
the Graduate College

ACKNOWLEDGMENTS

There are many who have helped me on this journey and I now have the opportunity to thank several of these people.

First, I would like to thank my supervisor and mentor Dr. Mirotznik. His guidance and steadfast encouragement proved invaluable in seeing me through to the finish. He had confidence in me from the beginning and I am humbled to have had the chance to work with him.

Austin Good, Zachary Larimore, Paul Parsons, Siddartha Garrett, Nick Hudak, Sarah Jensen, and Aric Lu inspired me daily with their knowledge and passion. I will not forget my time spent with them and I daresay we succeeded in our goal to “build cool stuff.” I also wish to thank Jenna Henke for proofreading this work and for making helpful suggestions and edits.

I must acknowledge the many men who have taught me much about football and about life. I owe special thanks to Coach Devine, Coach McCorkle, and Coach Polin. Lessons learned concerning mental-toughness, self-discipline, and perseverance proved valuable in writing this paper.

I would like to articulate my gratitude to my family. Words fail to express my affection for you all. For the many sacrifices you have made, the lessons you taught me, and the times you have lifted my spirit, I am thankful.

Finally, I thank my Lord and Savior Jesus Christ. Who can find a friend so faithful to journey through this life with. To God be the glory. Creation truly sings of His greatness.

Psalm 19: 1-4

“The heavens declare the glory of God; the skies proclaim the work of his hands.

Day after day they pour forth speech; night after night they reveal knowledge.

They have no speech, they use no words; no sound is heard from them.

Yet their voice goes out into all the earth, their words to the ends of the world.”

TABLE OF CONTENTS

LIST OF TABLES	vii
LIST OF FIGURES	viii
ABSTRACT	x

Chapter

1	INTRODUCTION	1
1.1	Motivation	1
1.2	Defining the Problem	2
1.3	Thesis Structure	3
1.4	Manufacturing Paradigms	4
1.4.1	Subtractive Manufacturing	4
1.4.2	Additive Manufacturing	5
1.4.2.1	Micro-dispensing	6
1.5	Materials	7
1.6	Antenna Theory	8
1.7	Antenna Transmission Line Analogy	11
1.8	Network Analyzer Basics	14
1.9	Antenna Parameters	15
1.9.1	Resonant Frequency	15
1.9.2	Antenna Efficiency	16
1.9.3	Directivity	17
1.9.4	Gain	17
2	FEEDBACK CONTROL IN ADDITIVE MANUFACTURING	19
2.1	Feedback Control	19
2.2	Closed-Loop Additive Manufacturing	21
2.3	Our Implementation of Feedback Control	23
2.3.1	Correcting for Errors	24
2.3.2	Detecting Steady State	27
2.3.3	Finding the Resonant Minimum	29
3	DESIGNING THE PATCH ANTENNA	31
3.1	Introduction to Microstrip Antennas	31

3.2	Modelling Approach.....	35
3.3	Analytical Model	36
3.4	Numerical Modeling.....	43
3.4.1	Building the 3D Model.....	44
3.4.2	Simulation Results.....	46
4	IMPLEMENTING THE CONTROL PROCESS.....	52
4.1	Overview	52
4.2	Preparing the Substrate.....	54
4.3	Control Interface Manual	54
5	CONCLUSION AND FUTURE WORK.....	59
5.1	Conclusion	59
5.2	Future Work.....	60
	REFERENCES	61

LIST OF TABLES

Table 3.1: Properties of conductor and dielectric materials used in the 3D model.....	44
Table 3.2: Comparison of the results from the analytical and numerical analysis. Notice that all units are given in mm.....	51

LIST OF FIGURES

<i>Figure 1.1: Micro-dispensing hardware schematic [12]</i>	<i>6</i>
<i>Figure 1.2: Measured and simulated transmission characteristics of copper and two conductive pastes [13].....</i>	<i>7</i>
<i>Figure 1.3: Antenna shown as a transition device, adapted from [16].</i>	<i>11</i>
<i>Figure 1.4: A transmission line terminated in load impedance. Adapted from [17]. ..</i>	<i>12</i>
<i>Figure 1.5: Two-port network with S-parameters defined in terms of incident and reflected voltage waves.</i>	<i>14</i>
<i>Figure 1.6: Keysight Technologies E8361C PNA Microwave Network Analyzer [19].....</i>	<i>15</i>
<i>Figure 1.7: Plot of S11 versus. frequency for a narrowband antenna. The resonant minimum is highlighted.</i>	<i>16</i>
<i>Figure 2.1: Block diagrams comparing the two types of control systems.....</i>	<i>19</i>
<i>Figure 2.2: Block diagram showing of the closed-loop feedback control system we employed to create a microstrip antenna.</i>	<i>24</i>
<i>Figure 2.3: Plot showing relationship between frequency resonant minimum and length of the patch antenna. The slope of the tangent line is shown for three frequencies considered in the design stage.</i>	<i>25</i>
<i>Figure 2.4: Plot of the magnitude of the reflection coefficient vs. frequency for twelve antennas of lengths differing by 0.1 mm. Made using HFSS.</i>	<i>27</i>
<i>Figure 2.5: Bock diagram showing the frequency sum of the squared differences between consecutive time samples.</i>	<i>28</i>
<i>Figure 3.1: The images above are reproduced from the works of Munson [29] and Gregorwich [30] and show the early applications of microstrip antennas.....</i>	<i>32</i>
<i>Figure 3.2: Rectangular microstrip patch antenna with variables labelled.</i>	<i>35</i>
<i>Figure 3.3: Flow diagram of the process used to generate G-code for the antenna. ..</i>	<i>36</i>
<i>Figure 3.4: Transmission-line model equivalent circuit. Modified from [16].</i>	<i>37</i>

<i>Figure 3.5: Cross section of (a) a microstrip transmission line, (b) its equivalent model using the effective dielectric constant, and (c) fringing of the electric field lines. Adapted from [16].</i>	38
<i>Figure 3.6: MATLAB plot of the effective permittivity as a function of microstrip trace width for three samples with varying substrate thicknesses.</i>	39
<i>Figure 3.7: Rectangular patch antenna with actual and effective lengths shown.</i>	40
<i>Figure 3.8: MATLAB code created to determine antenna dimensions</i>	43
<i>Figure 3.9: The three models developed in HFSS while designing the antenna.</i>	46
<i>Figure 3.10: HFSS automatic adaptive meshing [38].</i>	47
<i>Figure 3.11: Smith chart showing sweep over inset length with length and width held constant. Markers show the 5 GHz points on each curve.</i>	49
<i>Figure 3.12: Visualizing fields in HFSS to verify antenna performance.</i>	50
<i>Figure 4.1: Setup devised to allow in-situ measurements to be taken. Created using Autodesk™ Fusion 360.</i>	52
<i>Figure 4.2: nScript 3Dn-300 system used for fabricating the patch antenna [39]</i>	53
<i>Figure 4.3: Process used to prepare the substrate. (a) shows the exposed substrate after etching and (b) shows the protective paint layer covering the ground plane being removed in the demasking process.</i>	54
<i>Figure 4.4: MATLAB control interface</i>	55
<i>Figure 4.5: Pane showing which S-parameter is measured and plotted.</i>	57
<i>Figure 4.6: Pane where user can set process and cycle tolerance parameters.</i>	57
<i>Figure 4.7: Pane showing the frequency range over which measurements are taken.</i>	58

ABSTRACT

In recent years several authors have noted the immense potential of additive manufacturing (AM) to create parts for radio frequency and microwave applications. At the present time, however, AM lacks the consistency and reliability needed to make end-use parts. Quality assurance is of particular importance in high frequency applications, where small variations in material and geometry can have significant effect on performance.

This paper outlines a procedure for introducing feedback control in AM through real-time sampling of the S-parameters. At the core of the process is an algorithm that monitors a part's performance as material is added incrementally and, via reference to a model, updates the print-path to achieve best results. The merit of feedback as applied to our scenario is its ability to correct for disturbances in the manufacturing environment and the effects of underlying hidden variables. The efficacy of the procedure developed in this paper is then demonstrated for the practical scenario of 3D printing a microstrip antenna designed to operate in the C band.

Chapter 1

INTRODUCTION

1.1 Motivation

Additive manufacturing (AM) has seen many advances in the past few decades. As machine accuracy has increased and costs have decreased, 3D printers have found use in many diverse applications. Recently several researchers have shown that AM can be used to fabricate radio frequency (RF) and microwave devices [1] – [8]. Though it is doubtful that AM will displace traditional printed circuit board (PCB) manufacturing there are a set of scenarios in which AM might be preferred. According to Jordan [9] AM has the ability to excel in the following four production scenarios:

- Short production runs such as prototypes or replacement parts
- High production complexity
- Highly customized items
- Spatially remote production

These factors are present in several RF applications. The high cost of RF components relative to other electronic components can be in part attributed to these qualities. Additive manufacturing has the potential to reduce costs and make feasible hereto unrealizable RF structures; however, prior to more widespread adoption several challenges must be overcome.

1.2 Defining the Problem

One of the most significant challenges facing additive manufacturing is the lack of consistency and reliability of printed parts. As a consequence of this, AM is typically avoided in highly sensitive applications that cannot tolerate risk. AM is often thought of as a “black box” procedure, creating an exact replica of a given model. The reality, as anyone who has used a 3D printer can testify, is much different and can vary from day-to-day. As a result, AM is as much of an art as it is a science, often requiring several trial prints to tune parameters to reach a desired geometry. Even the highest quality machines produce parts with some variability despite identical inputs. As printers continue to improve in precision and account for variability in material and environmental effects these effects will be mitigated. However, there exists a deeper and even more elusive source of error inherent in the AM process.

In the current product development lifecycle CAD software is nearly universally employed by engineers to refine designs and simulate behavior under a variety of input conditions, whether those be mechanical, thermal, or electrical. The problem is that these software design tools model 3D objects as homogeneous, and not as a series of layers. The structural properties of an object made through deposition of a series of layers, even with a post processing phase, will be different than the case in which subtractive manufacturing is applied to a homogenous slab of material. One might ask, why if these slicing effects are truly important can't they simply be built into the design software. This is certainly a reasonable solution, except that these effects are not well known and vary from printer-to-printer and over time. As investigators continue to explore the fundamental science of how materials behave in the AM process there is little doubt that more accurate models, methods of characterization, and test standards will emerge and be incorporated into the software

design packages used by practicing engineers. *In the meantime, there is another solution that employs real-time feedback and control to adjust printing processes on the fly to consistently produce high quality parts.* It is the goal of this thesis to explain this approach for the general case as well as for the particular case of fabricating electromagnetic structures.

1.3 Thesis Structure

The work presented in this thesis relies on a synthesis of research and technology coming from the following domains: control systems, electromagnetics, manufacturing, and materials science. In an effort to be comprehensive and make our work accessible to a wider audience the remainder of this chapter is devoted to providing important definitions and background material. The reader familiar with this material already is encouraged to move ahead to the second chapter.

Chapter 2 introduces the closed-loop additive manufacturing (CLAM) process. The general approach is introduced as an eight-step process. Important considerations for each step are described in detail. After laying the theoretical framework, the final section discusses the use of the CLAM process to fabricate an antenna with properties that more closely resemble those specified by the designer.

Chapter 3 is concerned with designing a patch antenna to be used in the CLAM process. It should be stressed that CLAM is not a replacement for the underlying engineering design concepts. A model needs to be developed to find dimensions for the initial print as well as the differential variation of the electromagnetic properties with respect to differential changes in geometry.

Chapter 4 presents the practical details involved in designing the closed-loop control interface and fabricating the antenna. The capabilities of the nScript printer

are described and the results from printing are summarized. The theory presented in Chapter 2 is referenced as we develop our algorithm. A manual explaining the

Chapter 5 summarizes the work presented in this thesis and presents a vision of the future research into how feedback control might be applied to AM. In the immediate future we envision how feedback-control might be expanded beyond fabricating antennas to fabricating other RF/Microwave structures. Advances in the fundamental disciplines that compose our work combined with vision and creative application of these results have potential to shape the future of manufacturing.

1.4 Manufacturing Paradigms

There are, in simplified terms, three ways of making things: subtraction, molding, and addition [9]. In this section an overview of the conventional subtractive manufacturing techniques used to produce RF and microwave components will be presented. A brief introduction to additive manufacturing will follow, with a focus on fabricating high frequency devices.

1.4.1 Subtractive Manufacturing

Traditionally, the PCB industry has relied on subtractive manufacturing in the form of *chemical milling*. Unlike classical milling, chemical milling (also called etching) uses chemicals to selectively remove material. The process has 5 steps [10]:

- 1) Cleaning
- 2) Masking
- 3) Scribing
- 4) Etching
- 5) Demasking

The process begins with cleaning, which is done to remove contaminants and prepare the surface to accept the maskant. Masking is the process of applying a coating that resists the etchant. Scribing is used to selectively remove portions of the masking to expose the metal underneath to an etchant. Etching places a chemical solution in direct contact with sample and causes the exposed portions of the sample to be removed. The rate of etching is dependent on the reaction taking place and a number of other environmental factors. Demasking is the final step whereby the remaining protective mask is removed from the part. Chemical milling, compared to classical milling, has the advantages of being able to produce complex geometries with high accuracy. A drawback of chemical milling is that the chemical byproducts created are often hazardous and require proper handling and disposal. Additive manufacturing seeks to offer similar accuracy to chemical milling all while reducing the material and chemical footprint of production.

1.4.2 Additive Manufacturing

The term *additive manufacturing* refers to the process by which a 3-dimensional object is constructed as material is added layer by layer. A variety of AM techniques have been applied to fabricate RF/Microwave components. Some of the more common methods explored include Fused Deposition Modeling (FDM), PolyJet, Micro-dispensing, Selective Laser Sintering (SLS), and Stereolithography (SLA).

The literature shows two approaches to making high frequency electromagnetic devices [11]. The first is to print plastic parts and make them conductive by means of a post-print metallization step. Metallization is typically accomplished using physical vapor deposition or electroplating. The second is to print conductive parts directly, through melting metal powders (as in SLS) or by curing a

conductive paste (as in micro-dispensing). The method of real-time feedback control as described in this paper cannot be implemented for the first case and therefore the second is used in our work. Parts produced using SLS typically have rough surfaces and require post-processing steps such as polishing or milling. Furthermore, there are formidable challenges to using SLS in multi-material prints. For these reasons micro-dispensing is perhaps the best choice for fabricating RF/Microwave structures, given the current state of technology.

1.4.2.1 Micro-dispensing

Micro-dispensing is a form of paste extrusion in which a small quantity of liquid, typically on the order of a fraction of a microliter, is deposited. Pneumatic pressure is used to regulate the flow of material to ensure precise deposition. Micro-dispensing systems can print materials with absolute viscosity, in units of centipoise (cP) within a certain range.

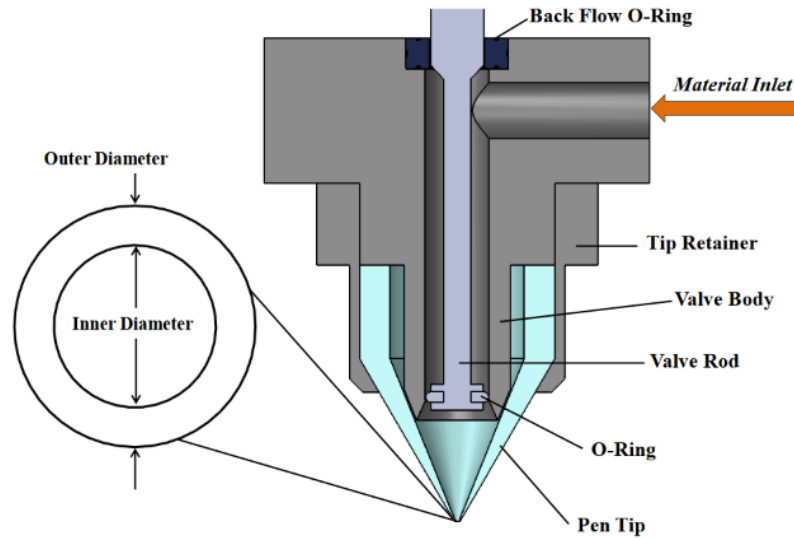


Figure 1.1: Micro-dispensing hardware schematic [12]

The micro-dispensing system used in this project, the nScript 3Dn-300, is described in greater detail in the fabrication section.

1.5 Materials

One of the chief challenges is using AM to create high frequency electromagnetic structures is the limited number of materials that are compatible with this fabrication method. This is an area of much active research and it is likely that time will produce a greater palette of materials. Conductive pastes compatible with micro-dispensing can be made by loading an organic binder with metallic flakes. Highly conductive materials are needed at RF/Microwave frequencies to ensure parts have high efficiency and do not experience significant ohmic losses. A conductivity study, completed by Good [13] was used to determine the paste that showed highest conductivity over frequencies ranging from 1-30 GHz. Transmission lines were fabricated, and transmission characteristics were measured. The results of the study are shown in Figure 1.2. As expected from simulations, the conductive pastes did not perform as well as bulk copper. KA801, a silver flake paste, was observed to have the best performance and was therefore the material selected for use.

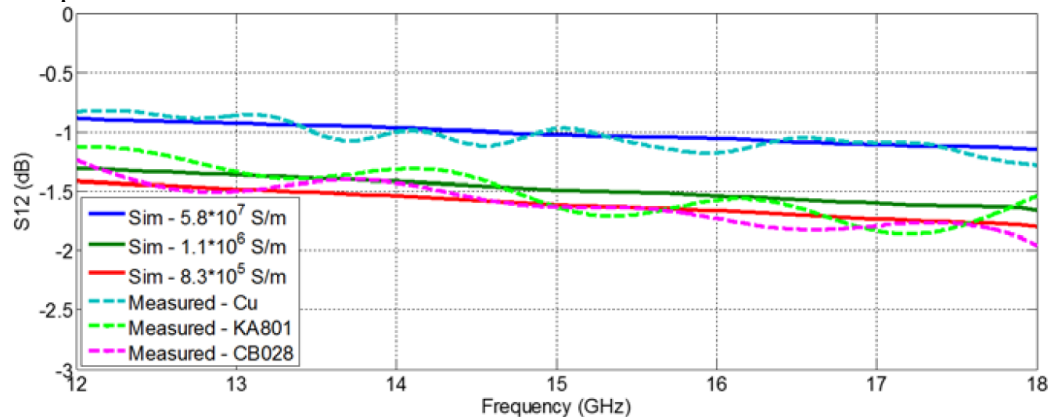


Figure 1.2: Measured and simulated transmission characteristics of copper and two conductive pastes [13]

1.6 Antenna Theory

According to the *IEEE Standard Definitions of Terms for Antennas* (IEEE Std 145—2013) [14] an antenna is “that part of a transmitting or receiving system that is designed to radiate or to receive electromagnetic waves.” Antennas come in a variety of shapes and sizes, which are chosen to satisfy a particular application. In this section we outline the fundamental mathematical theory of electromagnetic waves and highlight some of the practical results relating to antennas. The approach used is based loosely on that found in [15] - [17].

During the nineteenth century a series of experiments led to the formulation of a set of laws known as Maxwell’s equations. These equations are foundational to the discipline of Electrical Engineering and in the language of mathematics are expressed as a set of four first-order partial differential equations [1].

$$\nabla \times \bar{\mathbf{E}} = -\frac{\partial \bar{\mathbf{B}}}{\partial t} - \bar{\mathbf{M}} \quad (1.1)$$

$$\nabla \times \bar{\mathbf{H}} = \bar{\mathbf{J}} + \frac{\partial \bar{\mathbf{D}}}{\partial t} \quad (1.2)$$

$$\nabla \cdot \bar{\mathbf{D}} = \rho_v \quad (1.3)$$

$$\nabla \cdot \bar{\mathbf{B}} = 0 \quad (1.4)$$

The quantities in bold represent time-varying vector fields that are functions of space and time and are defined as follows:

$\bar{\mathbf{E}}$ = electric field intensity (volts/meter)

$\bar{\mathbf{H}}$ = the magnetic field intensity (amperes/meter)

$\bar{\mathbf{D}}$ = the electric flux density (coulombs/square meter)

$\bar{\mathbf{B}}$ = magnetic flux density (webers/square meter)

$\bar{\mathbf{M}}$ = the impressed (source) magnetic current density (volts/square meter)

$\bar{\mathbf{J}}$ = the electric current density (amperes/square meter)

ρ_v = electric charge density (coulombs/cubic meter)

Maxwell's equations describe the behavior of electric and magnetic fields at a macroscopic level and postulate the existence of electromagnetic waves. It would be more than a decade later before Maxwell's theory of electromagnetic waves would be experimentally verified by German professor Heinrich Hertz.

In order to solve Maxwell's equations, we must realize that these equations are coupled first-order partial differential equations. Thus, the approach we will take to decouple these equations is to increase the order. The mathematical expression that results is a second-order partial differential equation known as the wave equation. We assume a source free and lossless media and take the curl of both sides of Equations (1-1) and (1-2).

$$\begin{aligned}\nabla \times \nabla \times \bar{\mathbf{E}} &= -\mu \nabla \times \left(\frac{\partial \bar{\mathbf{H}}}{\partial t} \right) \\ &= -\mu \frac{\partial}{\partial t} (\nabla \times \bar{\mathbf{H}})\end{aligned}\tag{1.5}$$

$$\begin{aligned}\nabla \times \nabla \times \bar{\mathbf{H}} &= \epsilon \nabla \times \left(\frac{\partial \bar{\mathbf{E}}}{\partial t} \right) \\ &= \epsilon \frac{\partial}{\partial t} (\nabla \times \bar{\mathbf{E}})\end{aligned}\tag{1.6}$$

Making use of the vector identity

$$\nabla \times \nabla \times \bar{\mathbf{F}} = \nabla(\nabla \cdot \bar{\mathbf{F}}) - \nabla^2 \bar{\mathbf{F}}\tag{1.7}$$

the left side of equations (1-5) and (1-6) can be expanded

$$\nabla(\nabla \cdot \bar{\mathbf{E}}) - \nabla^2 \bar{\mathbf{E}} = -\mu \frac{\partial}{\partial t} (\nabla \times \bar{\mathbf{H}})\tag{1.8}$$

$$\nabla(\nabla \cdot \bar{\mathbf{H}}) - \nabla^2 \bar{\mathbf{H}} = \epsilon \frac{\partial}{\partial t} (\nabla \times \bar{\mathbf{E}})\tag{1.9}$$

From equations (1-3) and (1-4) we notice that the leftmost term of (1-8) and (1-9) drops out. We can now substitute in (1-1) and (1-2) to solve for

$$\nabla^2 \bar{\mathbf{E}} = \mu\epsilon \frac{\partial^2 \bar{\mathbf{E}}}{\partial t^2} \quad (1.10)$$

$$\nabla^2 \bar{\mathbf{H}} = \mu\epsilon \frac{\partial^2 \bar{\mathbf{H}}}{\partial t^2} \quad (1.11)$$

These are the vector wave equations describing time-varying fields in a source-free ($\bar{\mathbf{J}} = \rho_v = 0$) and lossless ($\sigma = 0$) media. It should be here pointed out that the speed of light is contained in these equations and is

$$c = \frac{1}{\sqrt{\mu\epsilon}} \quad (1.12)$$

In free-space $c_0 = 2.998 \times 10^8$ meters per second. The wave equation is common in the physical sciences and its solutions are readily found. Working in a rectangular coordinate system the general solution is

$$f(z, t) = F_1(z - ct) + F_2(z + ct) \quad (1.13)$$

Or equivalently,

$$f(z, t) = F_1(kz - \omega t) + F_2(kz + \omega t) \quad (1.14)$$

Where $c = \omega/k$. The phase constant is k and the angular frequency is ω . Equations (1-13) and (1-14) can be easily verified through direct substitution into (1-10) or (1-11). To an observer at rest the wave retains the shape it has initially at $t = 0$, but propagates in the z -direction with a speed c . At the time these results were profound.

The preceding discussion has established that electromagnetic radiation is a wave, and thus should exhibit certain properties common to all waves. The principle of superposition and constructive and destructive interference are of particular significance and deserve mention here. Additionally, as is known from classical mechanics, the velocity of a wave is the product of its wavelength and frequency.

$$c = \lambda f \quad (1.15)$$

Waves of different frequencies have unique energies and interact with matter differently.

1.7 Antenna Transmission Line Analogy

The wave nature of electromagnetic radiation has been discussed in the previous section and here we will explore the mechanisms by which such waves arise and are transmitted over free space. Radiation arises due to an accelerating (or decelerating) charge. Since current is related to charge by

$$I = \frac{dQ}{dt} \quad (1.16)$$

an equivalent condition for radiation is that there exists a time-varying current. Figure 1.3. illustrates the way in which this current is delivered to an antenna. A source generates a time-varying current, which is fed via a transmission line to the antenna. This diagram is particularly helpful because it introduces a new mode of thought whereby we can approach the subject of antennas. Namely, an antenna may be thought of as an impedance transformation device that matches the characteristic impedance of the transmission line (typically $50 \, \Omega$) to the impedance of free-space (about $377 \, \Omega$). In the following section the basics of transmission line theory will be reviewed.

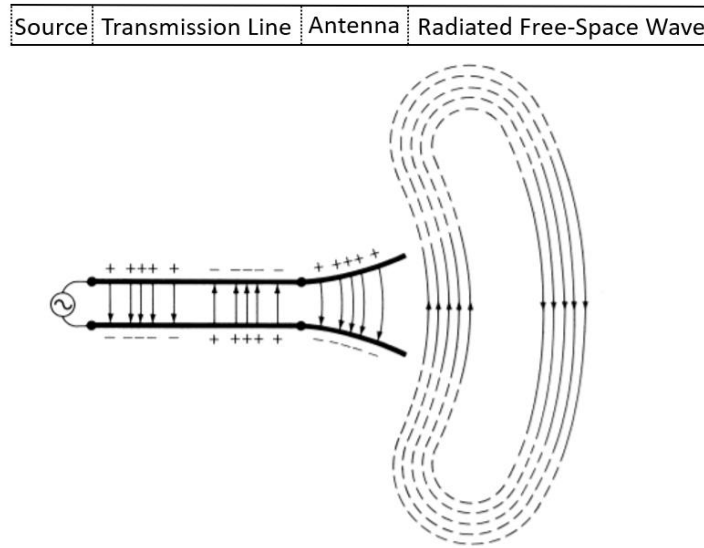


Figure 1.3: Antenna shown as a transition device, adapted from [16].

Wave propagation in a transmission line can be viewed as a specialized case of Maxwell's equations. Instead of working with the vector electric and magnetic fields it is typical to consider the scalar voltage $V(z)$ and current $I(z)$ on the line. For the case of a lossless transmission line the general solution can be written [17]

$$V(z) = V_0^+ e^{-jkz} + V_0^- e^{+jkz} \quad (1.17)$$

$$I(z) = \frac{V_0^+}{Z_0} e^{-jkz} - \frac{V_0^-}{Z_0} e^{+jkz} \quad (1.18)$$

where now the phase constant is

$$k^2 = \omega^2 LC \quad (1.19)$$

And the characteristic impedance is defined in terms of the series inductance per unit length and shunt capacitance per unit length.

$$Z_0 = \sqrt{\frac{L}{C}} \quad (1.20)$$

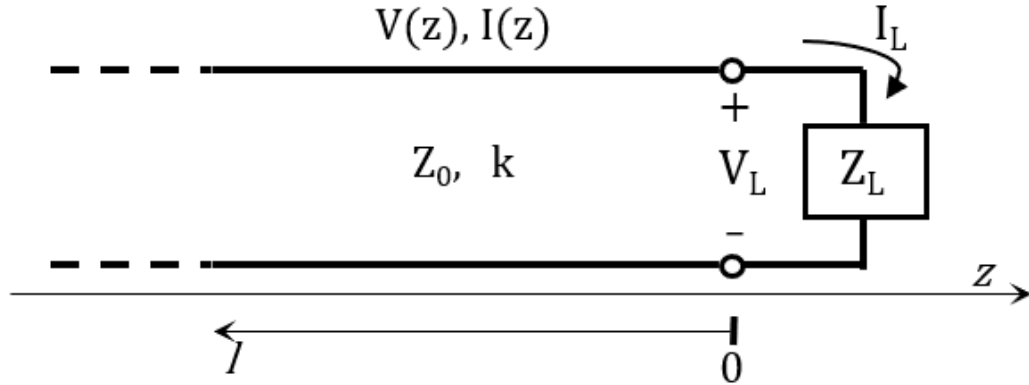


Figure 1.4: A transmission line terminated in load impedance. Adapted from [17].

Consider now a terminated lossless transmission line as shown in Figure 1.4. In this case the load is analogous to our radiating antenna. To the left is a source that

emits initially only a forward travelling wave. When this forward travelling wave encounters the load a portion of the voltage will be reflected. We define *the reflection coefficient*, Γ , as the ratio of the magnitude of the backward travelling wave that of the forward travelling wave.

$$\Gamma = \frac{V_0^-}{V_0^+} = \frac{Z_L - Z_0}{Z_L + Z_0} \quad (1.21)$$

In other words, the reflection coefficient is a measure of how much of the incident wave is reflected when encountering a load. The reflection coefficient will prove to be a valuable quantity for determining the efficiency of our antenna as will be discussed later.

The total voltage on the line can now be written as a sum of the forward and backward travelling waves. From (1-21) we see that the magnitude of the voltage of the backward travelling wave is simply the product of the magnitude of the voltage of the forward travelling wave and the reflection coefficient. Plugging into (1-17) and (1-18) at $z = -l$ yields

$$V(-l) = V_0^+(e^{+jkl} + \Gamma e^{-jkl}) \quad (1.22)$$

$$I(-l) = \frac{V_0^+}{Z_0}(e^{+jkl} - \Gamma e^{-jkl}) \quad (1.23)$$

The impedance seen looking into the line varies with position and the impedance at $z = -l$ is

$$Z_{in} = \frac{V(-l)}{I(-l)} = Z_0 \frac{V_0^+(e^{+jkl} + \Gamma e^{-jkl})}{V_0^+(e^{+jkl} - \Gamma e^{-jkl})} = \frac{1 + \Gamma e^{-2j\beta l}}{1 - \Gamma e^{-2j\beta l}} Z_0 \quad (1.24)$$

This can be written in a more useful form through plugging in (1-21) and simplifying:

$$Z_{in} = Z_0 \frac{Z_L + jZ_0 \tan(\beta l)}{Z_0 + jZ_L \tan(\beta l)} \quad (1.25)$$

Notice that when $l = \lambda/2$ Equation (1-25) reduces to $Z_{in} = Z_L$. This result will be important in future discussion.

1.8 Network Analyzer Basics

Abstraction is a familiar concept to most scientists and engineers.

Understanding the internal dynamics of a system is often of less importance than knowing how the system responds to a given input. A network analyzer allows for characterization of the behavior of a complex system at high frequencies through introducing what are called *scattering-parameters* or S-parameters for short.

For our purposes S-parameters must be used, as opposed to the low-frequency Z- or Y-parameters, because at high frequencies the net voltage is a combination of two or more traveling waves [18]. Due to the linearity of Equations (1-1) to (1-4) and the linearity of most microwave devices, the reflected and transmitted wave amplitudes are linearly related to the incident wave amplitude.

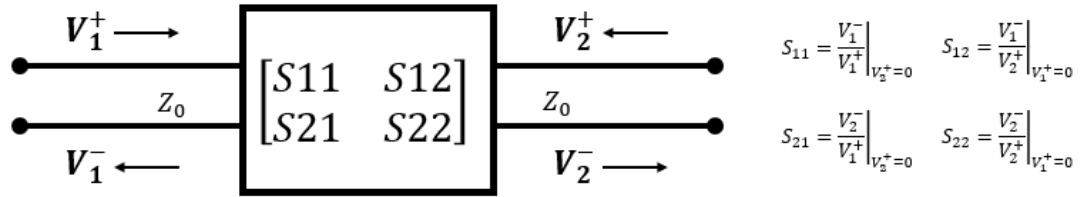


Figure 1.5: Two-port network with S-parameters defined in terms of incident and reflected voltage waves.

A two-port network is shown in Figure 1.5. If the characteristic impedances at all ports is the same the following matrix equation can be used to relate the incident and reflected waves.

$$\begin{bmatrix} V_1^- \\ V_2^- \end{bmatrix} = \begin{bmatrix} S_{11} & S_{12} \\ S_{21} & S_{22} \end{bmatrix} \begin{bmatrix} V_1^+ \\ V_2^+ \end{bmatrix} \quad (1.26)$$

In general S-parameters are a function of frequency. A network analyzer is designed to display S-parameters only over a limited range of frequencies. The network analyzer

used in our experiments is a Keysight Technologies E8361C Programmable Network Analyzer which can measure frequencies from 10MHz to 67GHz. Calibrations were done using the 85052D 3.5 mm calibration kit.



Figure 1.6: Keysight Technologies E8361C PNA Microwave Network Analyzer [19]

1.9 Antenna Parameters

In the previous sections we have discussed what an antenna is and the tool used to characterize these devices. This section will present important definitions and parameters that will be relevant when we design our antenna.

1.9.1 Resonant Frequency

Antennas are frequency sensitive devices. The *resonant frequency* of an antenna is the point in the frequency domain at which an antenna transmits (or by reciprocity accepts) the greatest power. Alternatively, this is the point at which the reflection coefficient, given in equation (1-21), is minimized. We see that this occurs when $Z_L - Z_0 = 0$ or by rearranging, when $Z_L = Z_0$. From (1-25) this occurs when $l = \lambda/2$. In this configuration the frequency dependent reactive components cancel, and the

antenna appears as a purely resistive element. Figure 1.7 shows how the location of the resonant frequency can be determined from a plot of the magnitude of the reflection coefficient.

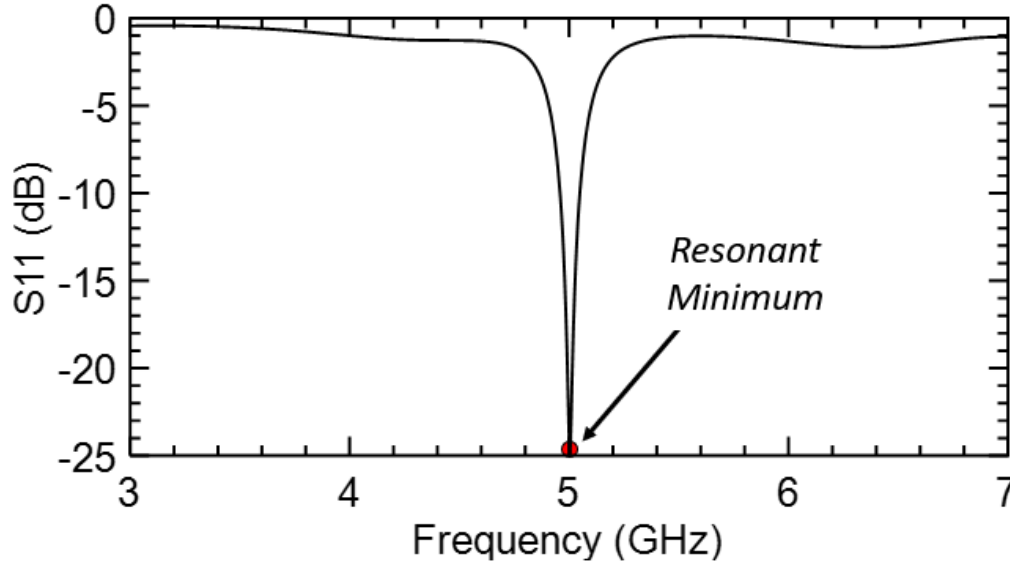


Figure 1.7: Plot of S_{11} versus. frequency for a narrowband antenna. The resonant minimum is highlighted.

The FCC has partitioned the electromagnetic spectrum into frequency bands [20]. Allocation of bands is done to prevent multiple transmitting antennas from broadcasting on the same channel and interfering with each other. The resonant frequency determines which band an antenna operates in and is therefore an important specification for the antenna designer.

1.9.2 Antenna Efficiency

Another important antenna parameter is its *efficiency*. A higher efficiency indicates more of the power supplied to the antenna is transmitted into space,

increasing the range of a communication system. Factors that diminish efficiency are called *losses*. Losses in an antenna can be attributed to one of the following three factors.

- Reflections due to mismatch
- Conduction losses
- Dielectric losses

An efficiency term can be assigned to each of the three factors above and the overall efficiency of the antenna can be expressed as the product

$$e_0 = e_r e_c e_d \quad (1.27)$$

The reflection mismatch efficiency can be calculated as $e_r = (1 - |\Gamma|^2)$. The conduction and dielectric efficiency, e_c and e_d , are determined experimentally.

1.9.3 Directivity

The *directivity*, D , of an antenna is the ratio of the radiation intensity in a given direction to the radiation intensity of an isotropic source. In spherical coordinates,

$$D(\theta, \phi) = \frac{U}{U_0} = \frac{4\pi U(\theta, \phi)}{P_{rad}} \quad (1.28)$$

P_{rad} is the total radiated power in watts. Often in practice, closed-form mathematical expressions are not available or are highly complex. In these cases, numerical methods can be applied.

1.9.4 Gain

The *gain* of an antenna is similar to the directivity but takes into account the antenna's efficiency. The gain is defined

$$G(\theta, \phi) = e_{cd} D(\theta, \phi) = e_{cd} \frac{4\pi U(\theta, \phi)}{P_{rad}} \quad (1.29)$$

The *absolute gain* can also be introduced. The absolute gain includes the reflection mismatch efficiency.

$$G_{abs}(\theta, \phi) = e_r G(\theta, \phi) = e_r e_{cd} D(\theta, \phi) = e_0 \frac{4\pi U(\theta, \phi)}{P_{rad}} \quad (1.30)$$

Gain is often expressed in decibels (dB). In Chapter 3 a 3D plot of the absolute gain will be shown for the antenna we designed.

Chapter 2

FEEDBACK CONTROL IN ADDITIVE MANUFACTURING

2.1 Feedback Control

In this chapter we will approach our additive manufacturing setup from the perspective of a systems engineer and discuss our method for introducing feedback.

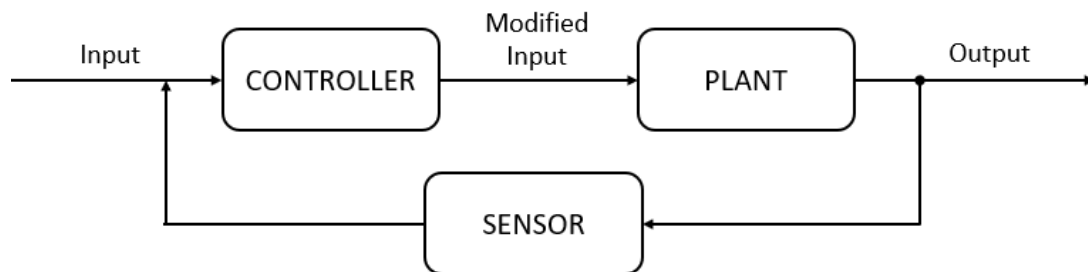
Control systems can be classified into one of two categories:

- Open-loop control
- Closed-loop control

Closed loop control is also commonly referred to as feedback control. The two types of systems are illustrated in Figure 2.1.



(a) Open-loop control



(b) Closed-loop control

Figure 2.1: Block diagrams comparing the two types of control systems.

The *plant* is defined as the part of the system we wish to control. In AM these are the motors and actuators that are used to position the printhead and control the rate at which material is deposited. Notice that in both open and closed-loop control there are system inputs and outputs. In AM the *input* is G-code or other numeric control instructions and the *output* is a 3D printed part. The difference between the two schemes is that in the closed-loop system the output is fed via a transducing element to a controller. In the *controller* the input is compared to the output and the degree to which the two differ, that is the *error*, is computed. The controller, through referencing a model, determines how the input ought to be modified such that the error term is minimized. According to Phillips and Parr [21] developing an appropriate model of the physical system accounts for 80 to 90 percent of the effort required in control-system analysis and design. The physical model we use will be presented in Section 2.3. and explained in greater detail in Chapter 3.

In a production scenario AM can be thought of as an open-loop procedure. Instructions are provided to the system which blindly follows them. At the conclusion of the print, an operator might put the output part through a visual inspection or other tests to verify it meets operational requirements. If the part does not satisfy requirements the operator will scrape away material or take other corrective action. If no such actions are possible the part is discarded and the model or print parameters are adjusted with the hope that the next print will yield better results. In this manner the operator is effectively acting as the feedback mechanism within this production system, however because feedback is not automated the overall process is not termed “closed-loop”.

2.2 Closed-Loop Additive Manufacturing

The term *closed-loop additive manufacturing* (CLAM) will be used to describe a distinct form of feedback control applied to additive manufacturing in a production scenario to improve the quality of parts. The process is comprised of the following steps:

- 1) Create model and specify properties of part
- 2) Identify which specifications the control system will target
- 3) Produce nearly the target value of the part
- 4) Add incrementally to the part
- 5) Take measurement
- 6) Compare to model and calculate error
- 7) Update print path to account for error
- 8) Repeat from step 3 until error is sufficiently small

The CLAM process begins like a typical AM process. A 3D CAD model is constructed for the part that will be created. A part will contain an assortment of metrics and specifications. Depending on the application, some of these metrics will have greater importance than others. In this stage the design engineer should rank the desired specifications in order of importance and decide which of these will be the subject of feedback control. Selection of a measurement system and controller will depend on the results from this step.

The next step is to fabricate the part. The model is sliced and G-code is provided to the controller. The controller sends instructions to the printer to print nearly the complete model of the part. The part is deliberately printed short of the desired value because we desire to use a strictly additive process. Additional material

can always be added if deemed necessary; however, if we overshoot the target value there is no way to make corrections without employing subtractive methods. By undershooting the desired performance specification, our controller can incrementally add geometry until desired performance is achieved. The size of the increments can be throttled as the desired value is approached to improve accuracy further.

After each increment is added to the part a measure is conducted to assess the effect. It is important that time be devoted to selecting an appropriate sensor and understanding its effects on the printed part. The selected measurement apparatus should not interrupt the print process and have no lasting effect on the part being measured. Sensors that meet these criteria are called *nondestructive*. According to the American Society for Nondestructive Testing (ASNT) there are fourteen forms of nondestructive testing [22], [23]:

- Magnetic Particle Testing
- Liquid Penetrant Testing
- Radiographic Testing
- Ultrasonic Testing
- Electromagnetic Testing
- Visual Testing
- Acoustic Emission Testing
- Guided Wave Testing
- Laser Testing Methods
- Leak Testing
- Magnetic Flux Leakage
- Neutron Radiographic Testing
- Thermal/ Infrared Testing
- Vibration Analysis

Acquired sensor data is used to correct the print path to account for errors. Mathematically, an error is defined as the absolute difference between the desired and measured parameter value, p , of the printed part.

$$error = |p_{desired} - p_{measured}| \quad (2.1)$$

The error is a metric that describes how far off the process is from achieving the end goal. After a measurement is taken the error is calculated. The question to be answered at that point is how to best respond to the error. Our model gives us an answer to this question. When we created the model earlier we also created a lookup table. The lookup table provides a one-to-one mapping between the value of the error term and the print action that should be taken. As the print process unfolds, if proper remedying actions are followed, the error should be observed to decrease. When the error passes below some predefined threshold the print process is done. That is, the print process is concluded when:

$$p_{desired} - p_{measured} < threshold_{process} \quad (2.2)$$

At this point the part should satisfy performance requirements within some set tolerance. It should be noted that the CLAM process integrates the typically post-processing quality assurance stage into the production process. Furthermore, because measurements are taken incrementally throughout the fabrication process more information is known about the part than in the case of post-production inspection.

2.3 Our Implementation of Feedback Control

This section will describe how the CLAM process was applied to fabricate a rectangular microstrip patch antenna. Figure 2.2 gives an overview of the major components and signals involved in the process. Feedback control will be applied to minimize the error in the location of the resonant frequency minimum. The significance of this parameter is discussed in Section 1.9. Notice that this parameter can be measured in real-time without effecting the print process (heating caused by exciting the antenna is negligible and can be safely ignored) through using a VNA.

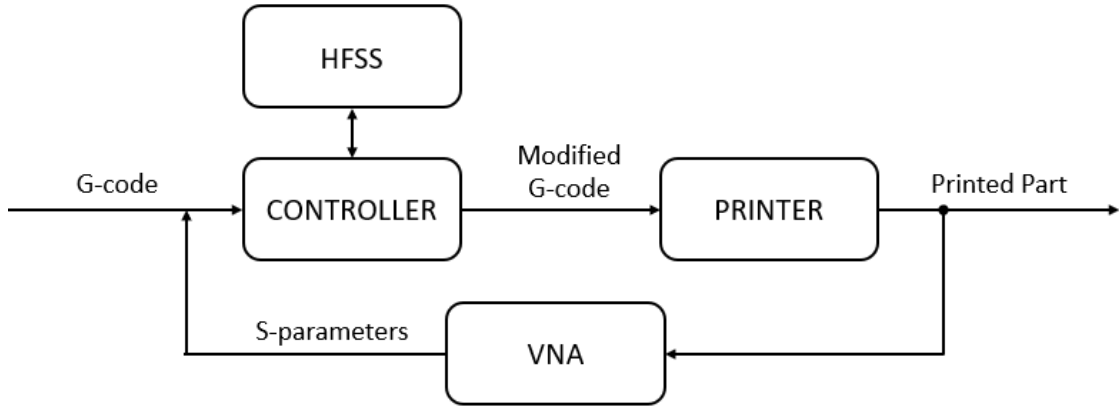


Figure 2.2: Block diagram showing of the closed-loop feedback control system we employed to create a microstrip antenna.

The controller extracts the resonant minimum from the measured S-parameters. The error is calculated and through referencing a model the print path of the next cycle can be determined such that the error is minimized. We will now discuss how we correct for errors in the print process.

2.3.1 Correcting for Errors

To correct for errors, it is important to first understand in what ways material might be added to the part such that errors are reduced. In Section 1.7 the importance of half-wavelength structures was discussed. It turns out that a microstrip antenna can be modeled by two radiating slots separated by a half-wavelength section of transmission line. For our purposes this means that the resonant frequency can be modified by simply extending the length of the antenna. In Chapter 3 we will find that the relationship between the resonant frequency, f_0 , and the length, L , of a microstrip antenna is

$$f_0 \approx \frac{c_0}{2L\sqrt{\epsilon_r}} \quad (2.3)$$

Though only approximate, this relationship will suffice for developing our control algorithm. A plot of this inverse relationship is shown in Figure 2.3. As the print process unfolds the length of the antenna increases and the resonant minimum decreases.

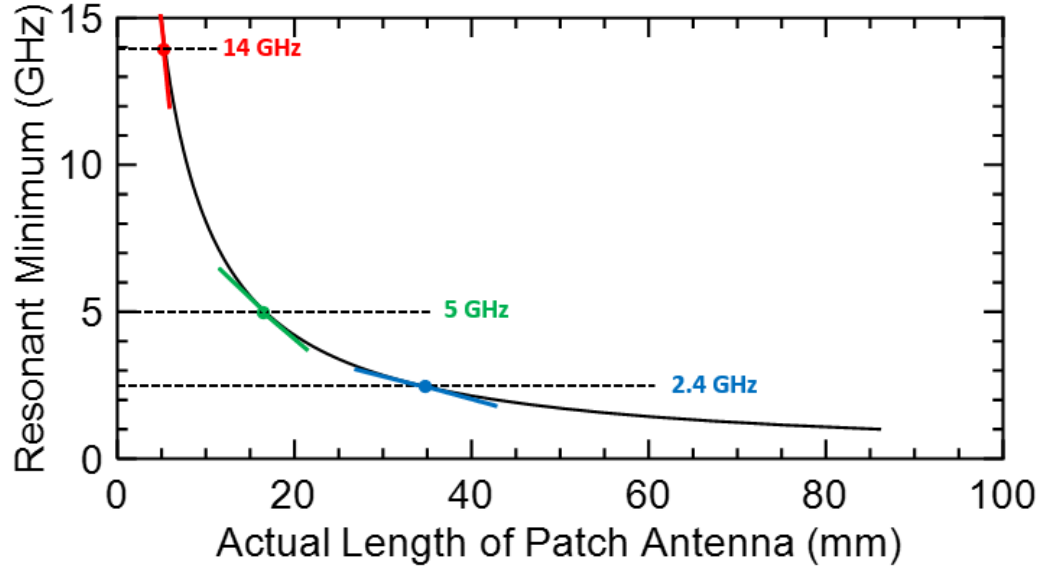


Figure 2.3: Plot showing relationship between frequency resonant minimum and length of the patch antenna. The slope of the tangent line is shown for three frequencies considered in the design stage.

To correct for errors, we must also select an appropriate process threshold as shown in Equation (2-2). The process threshold is used to decide whether to proceed with the next cycle or not and should be related to the smallest realizable frequency differential. Selecting an appropriate process threshold will ensure maximal accuracy is achieved while avoiding overshooting the desired resonant minimum. The frequency differential can be approximated,

$$\Delta f_0 \approx \frac{df_0}{dL} \cdot \Delta L = \frac{d}{dL} \left[\frac{c_0}{2L\sqrt{\epsilon_r}} \right] \cdot \Delta L = -\frac{c_0}{2L^2\sqrt{\epsilon_r}} \cdot \Delta L \quad (2.4)$$

Where L is the length at the resonant frequency and ΔL is the length the antenna is extended. The approximation of (2-4) is valid in the linear region, or in other words if ΔL is small. Figure 2.3 shows the slopes at three resonant frequencies to illustrate this idea. Notice that the steepness of the slope decreases as L increases. This indicates that for small antennas (high resonant frequency) a small addition in length has a much greater shift in resonant frequency than an equal addition of length would have for a larger antenna (lower resonant frequency). The 14 GHz antenna was initially considered, however upon further examination we determined it was not a suitable choice given the minimum line width of the nScript printer. The line width of the printer is the minimum unit of length that can be added to the antenna, ΔL . The nScript has a minimum line width on the order of 0.1 mm and thus the minimum differential frequency is found to be $\Delta f_0 = 226$ MHz for a resonant frequency $f_0 = 14$ GHz. At a resonant frequency $f_0 = 5$ GHz, the differential frequency is found to be $\Delta f_0 = 29$ MHz. This CLAM process guarantees that the printed antenna will have resonant frequency $f_0 \pm \Delta f_0$. The accuracy can be further improved by using a printer that can print smaller line widths.

As will be discussed in Chapter 3, numerical simulations were run in HFSS to validate results. The seven cycles leading up to the desired length are shown in Figure 2.4 spaced by ΔL , the line width of the nScript. HFSS numerical simulation show good agreement with the calculated frequency differential. Δf_0 was found to be on average 25.7 MHz.

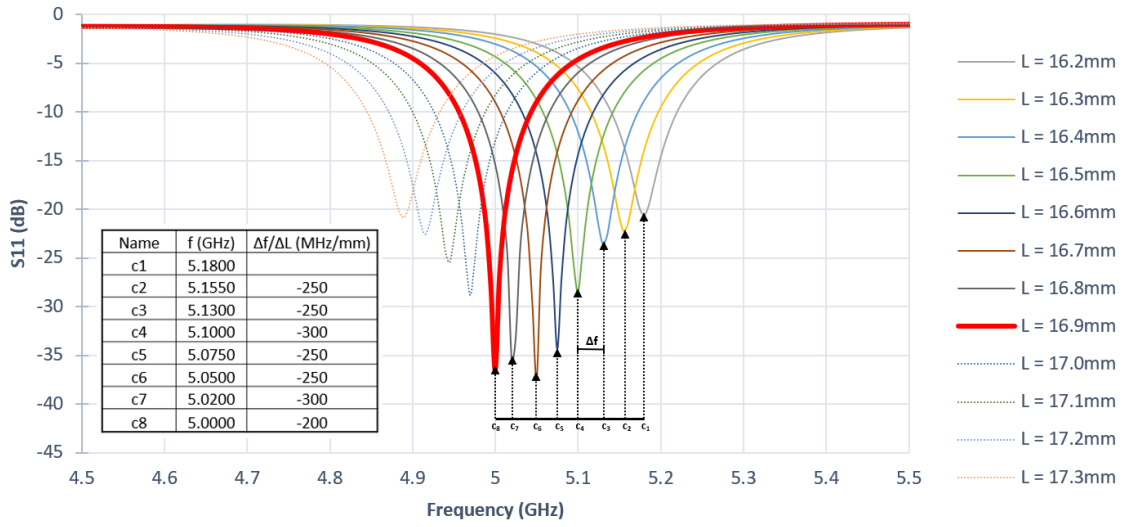


Figure 2.4: Plot of the magnitude of the reflection coefficient vs. frequency for twelve antennas of lengths differing by 0.1 mm. Made using HFSS.

2.3.2 Detecting Steady State

The process of printing the antenna can be thought of as a series of several cycles. A cycle begins when a line is added and ends when the resonant frequency has been determined. By adding material in each cycle, the antenna's resonant minimum is slowly shifted toward the desired resonant minimum as shown in Figure 2.4. However, when material is added to the antenna it does not instantaneous reach the its final state. This section will develop this idea and explain the method used to detect when the system has reached its steady state.

The network analyzer is setup to return the magnitude of S11 for N samples at frequencies ν spanning from f_{min} to f_{max} . The magnitude of the reflection coefficient is defined by the function

$$S(\nu, c, t) \quad (2.5)$$

Where c is an integer representing the current print cycle. The variable t indicates how much time has elapsed since the last print increment was completed. The variable t must be included because the conductive paste used in micro-dispensing does not reach its final conductivity instantaneously. A steady state is only reached after sufficient time has been allotted for the paste's organic binding compounds to decompose [24]. In steady state, Equation (2-5) can be described mathematically as

$$\lim_{t \rightarrow \infty} S(v, c, t) \quad (2.6)$$

Since it is of interest to minimize the time the print takes, and hence the time between print cycle incrementations, our control system should include functionality that detects when a steady state has been reached. The approach used is to sum the squared difference between consecutive samples in time.

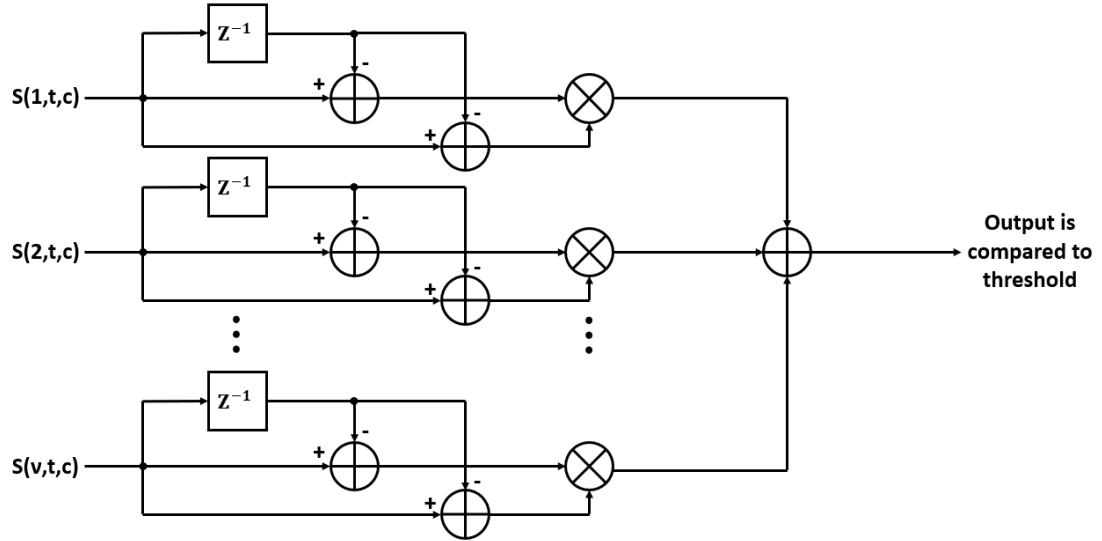


Figure 2.5: Block diagram showing the frequency sum of the squared differences between consecutive time samples.

As the process evolves toward steady state the sum of the differences squared will approach a constant value, the noise floor. By setting the cycle threshold just above this floor the steady state can be detected.

$$\sum_{v=f_{min}}^{f_{max}} [S_t(v, c) - S_{t-1}(v, c)]^2 < threshold_{cycle} \quad (2.7)$$

Equation (2-7) is depicted diagrammatically in Figure 2.5.

To improve the ability to sense when the cycle has entered steady state an averaging technique was employed. Averaging is commonly employed in fields such as radar and communications to increase the signal-to-noise ratio (SNR) of a signal [25]. Equation (2-7) is used but with the time samples replaced with their averages for τ samples

$$S_t(v, c) \rightarrow \frac{1}{\tau} \sum_{t=\frac{\tau}{2}-1}^{\tau} S_t(v, c) \quad (2.8a)$$

$$S_{t-1}(v, c) \rightarrow \frac{1}{\tau} \sum_{t=1}^{\frac{\tau}{2}} S_t(v, c) \quad (2.8b)$$

Plugging (2-8a) and (2-8b) into (2-7) gives

$$\sum_{v=f_{min}}^{f_{max}} \left[\frac{1}{\tau} \sum_{t=\frac{\tau}{2}-1}^{\tau} S_t(v, c) - \frac{1}{\tau} \sum_{t=1}^{\frac{\tau}{2}} S_t(v, c) \right]^2 < threshold_{cycle} \quad (2.8)$$

Notice that equation (2.8) is valid only if t is an even integer.

2.3.3 Finding the Resonant Minimum

This chapter will give details behind how the resonant minimum, $p_{measured}$, from Equation (2-2) is determined. The VNA does not directly provide the location of the resonant minimum, but rather this must be extracted from the S-parameters. Due to

sampling, the function measured is not analog but rather discrete. Mathematically, the comb function is used to describe the measured data.

$$comb[S(v, t, c)] = \sum_{k=-\infty}^{\infty} S(v, c, t) \delta(v - kF) \quad (2.7)$$

Where F is the spacing between consecutive samples and N is the number of samples.

$$F = \frac{f_{max} - f_{min}}{N} \quad (2.8)$$

Since we are confined to a finite bandwidth the sampled function shown in Equation (2-7) above must be multiplied by a rectangular function:

$$rect\left[\frac{v - f_0}{f_{max} - f_{min}}\right] \cdot comb[S(v, c, t)] \quad (2.9)$$

$$= rect\left[\frac{v - f_0}{f_{max} - f_{min}}\right] \cdot \sum_{k=-\infty}^{\infty} S(v, c, t) \delta(v - kF) \quad (2.10)$$

The location of the resonant minimum is our parameter of interest. Using our previous notation

$$p(v, t, c) = min\left(rect\left[\frac{v - f_0}{f_{max} - f_{min}}\right] \cdot \sum_{k=-\infty}^{\infty} S(v, c, t) \delta(v - kF) \right) \quad (2.11)$$

This equation shows that the measured resonant minimum will not be the ideal, or the minimum of the function $S(v, c, t)$. Rather, the measured location of the minimum will depend on the sampling scheme employed. A practical consequence of this section to the production engineer wishing to employ CLAM is that care must be taken in selecting the sampling rate and the interval over which sampling is done.

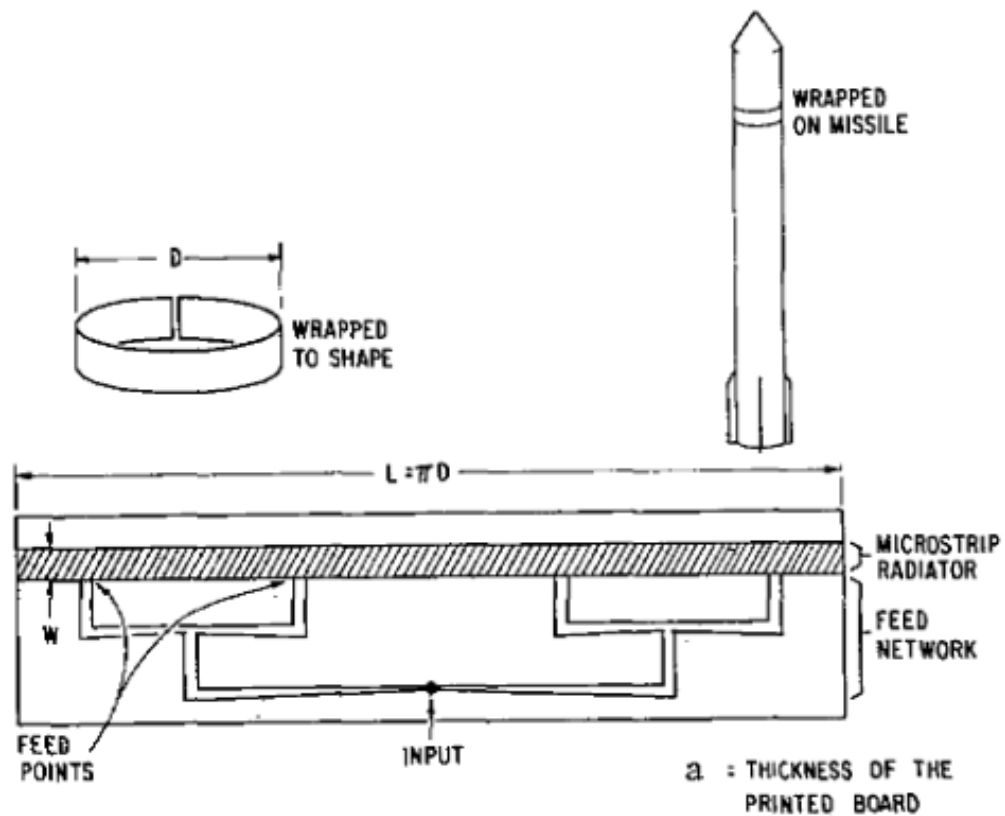
Chapter 3

DESIGNING THE PATCH ANTENNA

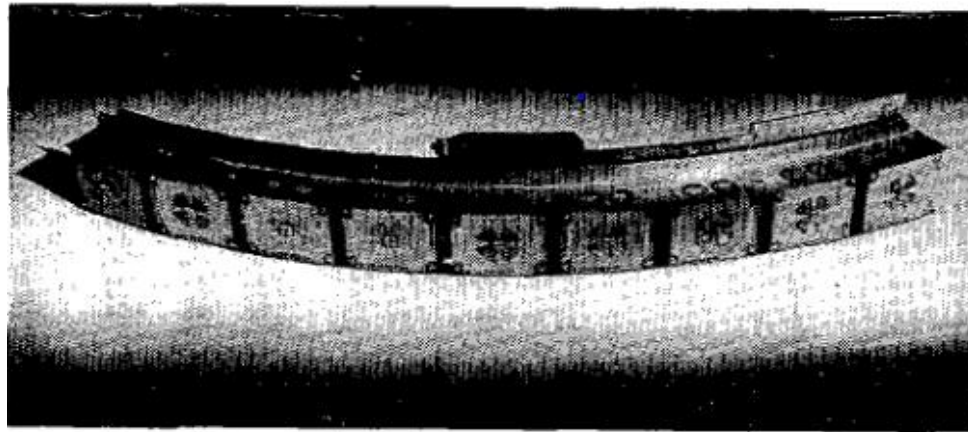
3.1 Introduction to Microstrip Antennas

Prior to the middle of the 20th century coaxial and twin-lead cables were the predominant means for transmitting radio frequency signals. Near the end of the Second World War investigators began to explore printed circuit board techniques and developed the stripline and microstrip transmission lines [26]. Early designers foresaw printed circuit board techniques as a means to mass produce cheaper microwave components. In an effort to reduce component losses the mechanisms of radiation were recognized and well appreciated [27], [28]. However, several years would elapse before researchers would recognize the vast potential of these low-profile antennas to meet a certain application need.

Interest in the microstrip antenna was revived in the early 1970's as a new generation of missiles was being developed and the need for a low-profile surface-conforming antenna became apparent. Figure 3.1 shows what is meant by a surface-conforming antenna and depicts the 1974 research efforts of Munson [29] and Gregorwich [30]. Part (a) of Figure 3.1 shows how a planar feed network and radiator can be wrapped around the cylindrical surface of a missile. Part (b) of Figure 3.1 illustrates a conformal array of crossed dipole etched microstrip elements to be flush-mounted on a cylindrical spacecraft. Despite some notable disadvantages the microstrip antenna was shown to be reliable and soon found additional use in high-performance aircraft and satellite applications.



(a) Wraparound microstrip antenna for use on a missile



(b) Conformal array for use on a spacecraft

Figure 3.1: The images above are reproduced from the works of Munson [29] and Gregorwich [30] and show the early applications of microstrip antennas.

The early 1980's was a period marked by an explosive growth in research focusing on the microstrip antenna and a corresponding increase in publications on the subject [31]. Analytic techniques that described the radiation characteristics and input-impedance characteristics for patch elements had come a long way and CAD techniques were developed to increase accuracy even further. Perhaps most importantly, the 1980's saw advances in the substrate and printing technology needed to make this antenna practically realizable. Though the patch antenna continued to be widely used in defense applications, civil sector markets have increasingly been a driving force behind modern research efforts [32]. In recent years microstrip antennas have found diverse application in areas such as the communication, biomedical, security, and automotive industries.

The widespread use of microstrip antennas can be attributed to the following desirable characteristics: [26], [27]

1. Advantageous mechanical and aerodynamic characteristics
2. Versatile electromagnetic characteristics
3. Ease of manufacturing

In high-velocity applications, such as in the case of aircraft, missiles, and rockets, it is desirable to have a low-profile and conformal radiator. Ideally a microstrip antenna can be added to the surface like a skin; disturbing neither aerodynamic flow nor the internal mechanical strength of the system [29]. Another important characteristic of microstrip antennas is that they come in many varieties and offer considerable design flexibility. Despite being confined to work within a plane and having only two degrees of freedom, the microstrip antenna designer has broad control over electromagnetic characteristics such as the radiation pattern, polarization,

input impedance, etc. In other words, the solution space, encompassing all 2D geometries fitting within some predefined board region, will include solutions that meet the needs of a diverse set of practical scenarios. As a simple example, circular polarization can be acquired through the appropriate addition of a second feed line to the radiating element. The final desirable attribute of microstrip antennas is that they take advantage of the accuracy and ease of printed-circuit board techniques. With photoetching techniques, the antenna can be fabricated on the same board as the rest of the circuit and other components can be easily integrated. Additionally, fabricating arrays made up of many radiating elements is made simple using these techniques.

The two most significant disadvantages of the microstrip antenna should also be mentioned. These are its narrow bandwidth and low efficiency [26]. The limited bandwidth arises due to the intrinsic high-Q resonator action in the thin substrate. Complicating the issue is that improved performance in one of these areas often comes at the expense of degradation in performance in the other. Factors such as humidity and temperature are also significant. Central to mitigating these harmful effects is proper selection of a stable, low-loss microwave substrate [27].

The subject of microstrip antennas is extensive and it is not our goal to give a comprehensive account. However, we do believe it is important to place our research in context and acknowledge, even if only briefly, the work done by those who came before us. Furthermore, we believe the success of the microstrip antenna, despite its disadvantages, provides a roadmap for the successful application of 3D printed antennas. Though 3D printed antennas are not likely to achieve equivalent performance as PCB antennas there are applications where they are superior and the

ability to create these antennas at the point of need may be the catalyst behind yet unforeseen technology.

3.2 Modelling Approach

The shape, size, and materials used in an antenna should be tailored to meet a particular performance goal. Microstrip antennas come in a variety of shapes and sizes. Square, rectangular, circular, elliptical, triangular are all valid configurations. The antenna we chose to design is a rectangular single feed microstrip patch antenna because it is common in practice and is well suited for verifying the closed-loop process discussed in Section 2.2. A rectangular patch antenna is shown in Figure 3.3 with several major variables labelled. It is our goal to now find a model that describes the effects of these variables on antenna parameters.

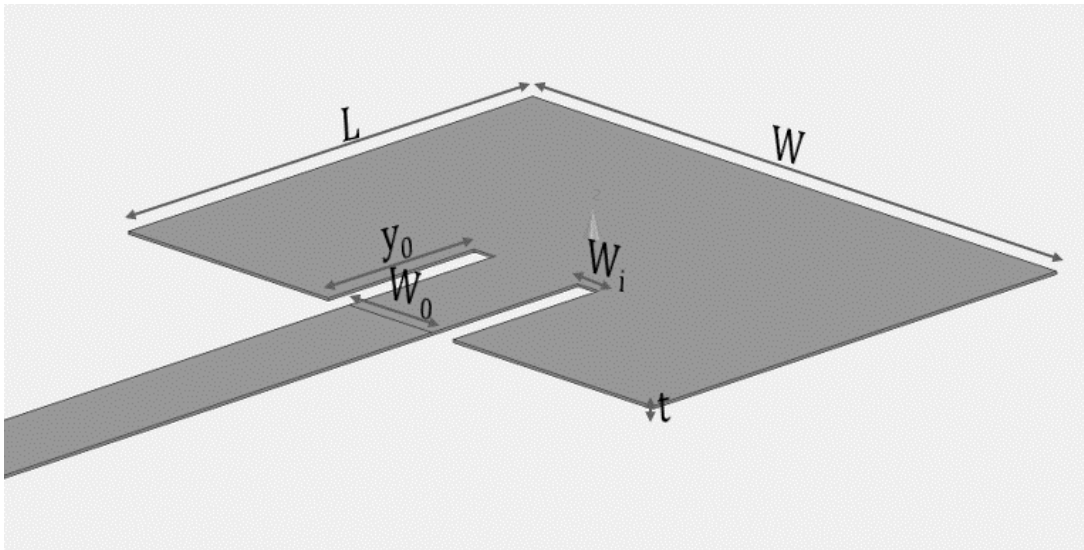


Figure 3.2: Rectangular microstrip patch antenna with variables labelled.

The design of the patch antenna was done using the process illustrated in Figure 3.3. First, an analytic method was used. The approach taken follows that described by Balanis and makes use of both the transmission-line and cavity models [15], [16]. The analytic method gives physical insight and is useful as a starting point; however, it fails to capture the full extent of the underlying physics. The results of the analytic method are used as an initial guess for a subsequent numerical method. HFSS, a commercial finite element method solver, was the computational electromagnetic tool selected to validate and further refine the analytic results. A 3D model is constructed, and parametric sweeps were run for several parameters. The 3D model is then converted to G-code which directs the print process during additive manufacturing.

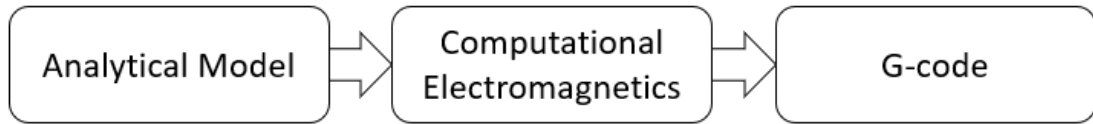


Figure 3.3: Flow diagram of the process used to generate G-code for the antenna.

3.3 Analytical Model

The transmission-line model is a typical starting point in the analysis of microstrip antennas. Though lacking accuracy this model yields considerable physical insight. It can be shown that a rectangular microstrip antenna can be represented by two radiating slots separated by a low-impedance transmission line, Z_c , of length L [33]. Each radiating slot has associated with it an impedance, Z_1 and Z_2 . Since the slots are in parallel with each other we write the impedance in terms of admittance where G is the conductance and B the susceptance [33]

$$Y = \frac{1}{Z} = G + jB \quad (3.1)$$

An equivalent circuit transmission-line model is shown in Figure 3.4. Since the two slots are identical, neglecting fringing effects associated with the feed point on slot 1, $G_1 = G_2$ and $B_1 = B_2$.

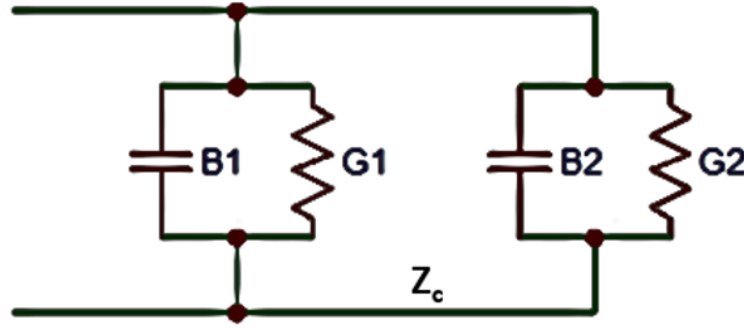


Figure 3.4: Transmission-line model equivalent circuit. Modified from [16].

It is now important to discuss the nature of the transmission-line of length L connecting the two radiating slots. The properties of transmission lines (discussed in section 1.7) hold but there are some additional points that must be mentioned. The type of transmission line that is the subject of our analysis is the microstrip transmission line. A microstrip transmission line, shown in Figure 3.5 (a), is made by depositing a conducting material above a ground plane separated by a low-loss dielectric substrate.

In the model we develop it is important to account for fringing because it effects the resonant frequency of the patch antenna. In fact, as will be seen later, this phenomenon is the reason why the resonant frequency is only approximately half a wavelength and not precisely half a wavelength as given in Equation (2-3).

Fringing occurs because the dimensions of length and width of the transmission line are finite. Figure 3.5 (c) illustrates fringing. Notice that toward the edges of the trace the electric field lines extend out further into the substrate before ending on the ground plane. The net effect of this is to make the microstrip trace look electrically wider than it truly is. Additionally, Figure 3.5 (c) shows that some electric field lines exist entirely within the substrate and some exist both within the air and substrate. Though for a well-designed microstrip transmission line, W/h and $\epsilon_r \gg 1$, most of the electric field lines travel in the substrate, the effect of the waves travelling in the air must be accounted for. This is done by introducing what is called the effective dielectric constant.

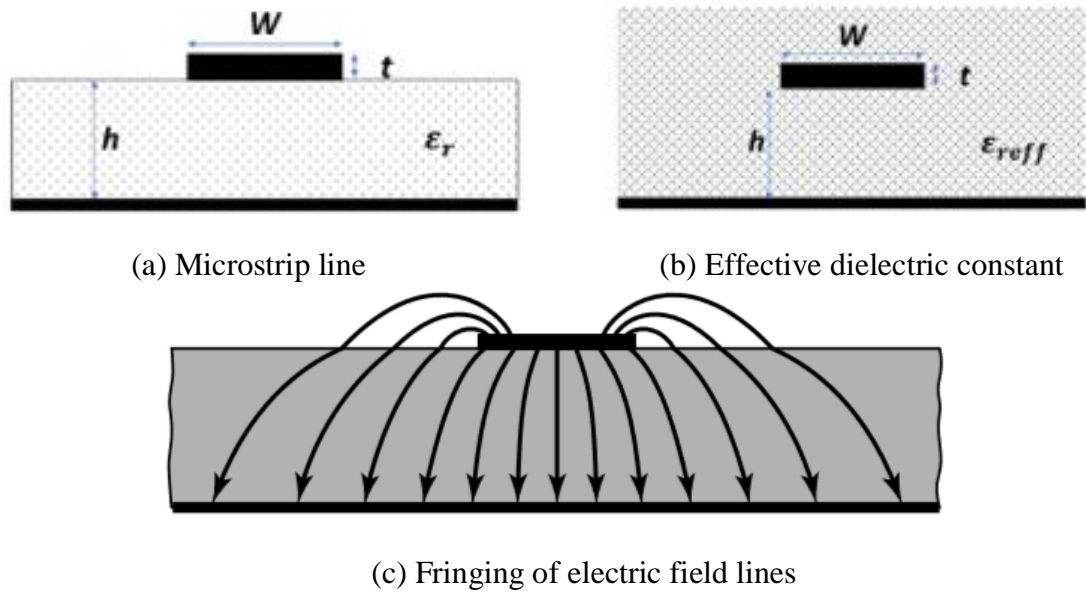


Figure 3.5: Cross section of (a) a microstrip transmission line, (b) its equivalent model using the effective dielectric constant, and (c) fringing of the electric field lines. Adapted from [16].

The effective dielectric constant accounts for wave propagation on the transmission line if the line were embedded entirely in a single homogeneous material, as shown in Figure 3.5 (b). The effective dielectric constant is [15]

$$\epsilon_{eff} = \frac{\epsilon_r + 1}{2} + \frac{\epsilon_r - 1}{2} \sqrt{\frac{1}{1 + 12 \frac{h}{W}}} \quad (3.2)$$

Figure 3.6 shows the predicted dependence of the effective permittivity on width for three samples of Rogers Board R03003 with different substrate thicknesses. Notice that in all cases the effective dielectric constant is always less than the actual dielectric of the substrate. Though as a designer we have flexibility over the width when printing we cannot change the substrate thickness, and thus it is important to pick a suitable substrate initially.

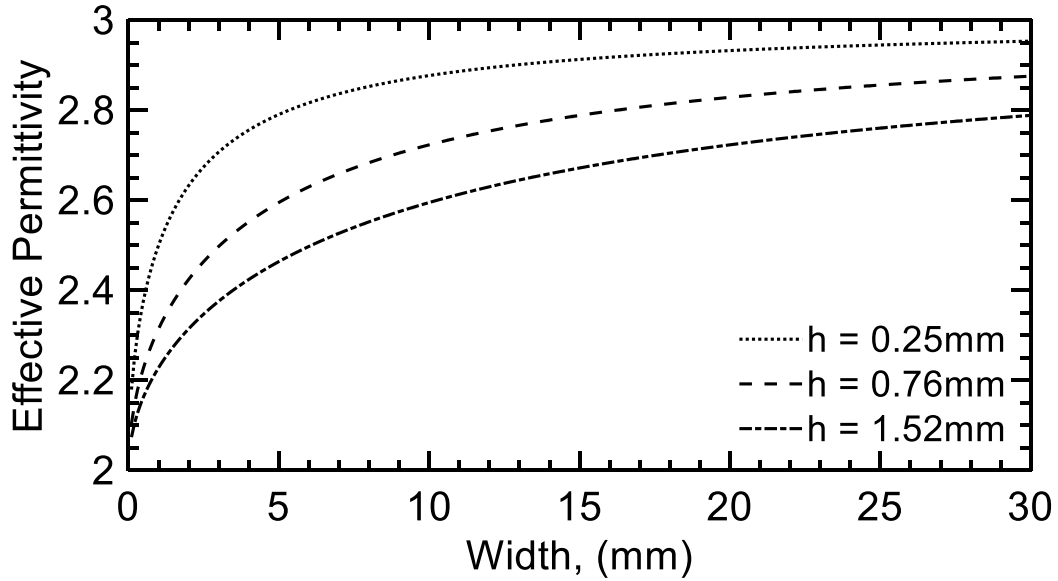


Figure 3.6: MATLAB plot of the effective permittivity as a function of microstrip trace width for three samples with varying substrate thicknesses.

Recall from Equation (1-25) that the actual length of a patch antenna is slightly less than half a wavelength as a result of fringing effects. A practical equation put forward by Johnson is [34]:

$$L \approx 0.49\lambda_d = 0.49 \frac{\lambda_0}{\sqrt{\epsilon_r}} = 0.49 \frac{c_0}{f_0 \sqrt{\epsilon_r}} \quad (3.3)$$

Balanis notes that the length will typically be somewhere in the interval $0.48\lambda < L < 0.49\lambda$ [16]. From Equation (3-3) we see that the length is inversely related to the dielectric constant within the length. This provides the inspiration for how we go about refining our model to further account for fringing effects. We have previously discussed that the net effect of fringing is to reduce the effective permittivity. By the reciprocal relationship of Equation (3-3) the net effect of a reduced effective permittivity is an increase in length of the antenna.

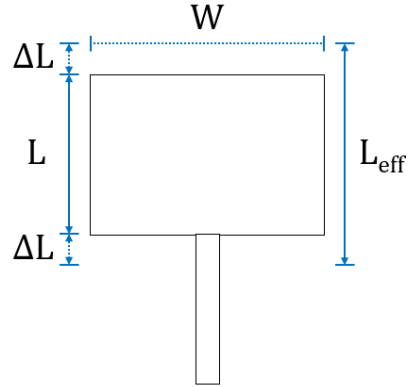


Figure 3.7: Rectangular patch antenna with actual and effective lengths shown.

To account for this in our model, we introduce an effective length, L_{eff} , in much the same way we introduced an effective permittivity.

$$L_{\text{eff}} = L + 2\Delta L \quad (3.4)$$

The extension in length of the patch antenna is a function of the effective permittivity. A practical and commonly used approximation for this extension in length is [16], [35]

$$\Delta L = 0.412 h \frac{(\epsilon_{reff} + 0.3) \left(\frac{W}{h} + 0.264\right)}{(\epsilon_{reff} - 0.258) \left(\frac{W}{h} + 0.8\right)} \quad (3.5)$$

Good radiation efficiencies can be achieved by using the width [16]

$$W = \frac{v_0}{2f_r} \sqrt{\frac{2}{\epsilon_r + 1}} \quad (3.6)$$

We are now in the position to determine the length and width of our antenna. The substrate thickness, h , and effective permittivity are determined by our selection of substrate material. We chose to work with Rogers Board™ R03003 of thickness $h = 0.76\text{mm}$ and dielectric constant $\epsilon_r = 3.00 \pm 0.04$. The frequency we chose was 5GHz. The length and width obtained from these specifications are $L = 17.07\text{mm}$ and $W = 21.21\text{mm}$.

In section 1.7 we discussed how an antenna may be viewed as the load of a transmission line. To maximize the efficiency of the antenna we must concern ourselves with impedance matching. Several techniques were considered:

1. Stub-matching
2. Quarter-Wavelength Transformer
3. Inset-feed Matching

The third choice was selected. We turn now to the cavity model to find the conductance of the first slot

$$G_1 = \frac{I_1}{120\pi^2} \quad (3.7)$$

where

$$I_1 = -2 + \cos(X) + X S_i(X) + \frac{\sin(X)}{X} \quad (3.8)$$

$X = k_0 W$ and the sine integral is given as:

$$S_i(X) = \int_0^X \frac{\sin x}{x} dx \quad (3.9)$$

The electrical separation between the two slots is half the wavelength of in the substrate $\lambda/2$, though due to fringing the actual length is less than this. If the proper distance is chosen, the susceptance of the second slot cancels completely with that of the first and the total resonant input admittance is real and equal to

$$Y_{in} = Y_1 + \tilde{Y}_2 = 2G_1 \quad (3.10)$$

The total resonant input resistance must also include the mutual effects between the two slots. The mutual conductance can be found.

$$G_{12} = \frac{1}{120\pi^2} \int_0^\pi \left[\frac{\sin\left(\frac{k_0 W}{2} \cos \theta\right)}{\cos \theta} \right]^2 J_0(k_0 L \sin \theta) \sin^3 \theta d\theta \quad (3.11)$$

Modifying Equation (3-10) and taking the reciprocal gives the expression for total resonant input resistance:

$$R_{in} = \frac{1}{2(G_1 \pm G_{12})} \quad (3.12)$$

Simplifying the expression in [36] and solving for the inset distance gives

$$y_0 = \frac{L}{\pi} \cos^{-1} \left(\sqrt{\frac{Z_0}{R_{in}}} \right) \quad (3.13)$$

Using the parameters specified above we find an inset length $y_0 = 6.20\text{mm}$ is needed to match to a line of characteristic impedance $Z_0 = 50\Omega$.

Code written in MATLAB to compute important dimensions following the method above is shown in Figure 3.8.

```

% Collin Wallish 3/27/19
% This script is used in the initial design of a patch antenna. The
% transmission line model is used and follows the method used by Balanis.

Eps_r = 3.00; % dielectric constant of the substrate = 3.00 +/-0.04
h_s = 0.76; % thickness of substrate (mm)
h_g = 0.035; % thickness of bottom cladding of substrate (mm)

% Constants
c0 = 3e11; % speed of light in a vacuum (mm/s)
f_r = (5e9); % resonant frequency (Hz)
lambda_0 = c0/f_r; % wavelength in vacuum (mm)
Z0 = 50; % desired input impedance (ohms)

% Calculate width of patch for an efficient radiator (mm)
W = (c0/(2*f_r))*sqrt((2/(Eps_r+1)));

% Calculate effective dielectric constant of the patch
Eps_reff = ((Eps_r+1)/2)+(((Eps_r-1)/2)*((1+(12*(h_s/W))))).^(-0.5));

% Calculate extended incremental length of the patch (mm)
dL = (h_s*0.412)*(((Eps_r+0.3)*((W/h_s)+0.264))/((Eps_r-0.258)*((W/h_s)+0.8)));

% Calculate the actual length of the patch antenna (mm)
L = (c0/(2*f_r*sqrt(Eps_reff)))-(2*dL);

% Calculate effective length of the patch antenna (mm)
L_eff = L + (2*dL);

% Calculate conductance of the 1st slot using the cavity model (siemens)
X = ((2*pi/lambda_0)*(W));
I1 = (-2)+(cos(X))+((X)*sinint(X))+ ((sin(X))/X);
G1 = I1/(120.*pi.*pi);

% Calculate mutual conductance in terms of far-zone fields
fun = @(x) (((sin((X/2)*cos(x)))/(cos(x))).^2).*(besselj(0,((2*pi*L*sin(x))/lambda_0))).*(sin(x)).^3);
G12 = (1/(120.*pi.*pi))*integral(fun,0,pi);

% Calculate the resonant input resistance
Rin = (1/(2*(G1+G12)));

% Calculate input feed distance from slot 1
y0 = (L/pi)*acos(sqrt(Z0/Rin));

```

Figure 3.8: MATLAB code created to determine antenna dimensions

3.4 Numerical Modeling

In this section we describe how the patch antenna and its feed are modeled in HFSS. The simulation results match well with the analytic model developed in the previous section. Further insight into the modes in the antenna and the antenna's far field behavior are achieved through the computational techniques used in this section.

3.4.1 Building the 3D Model

The first step in the simulation process was to construct a 3D model in HFSS. Parametric modeling, as opposed to direct modeling, was used. Parametric modeling allows a shape to be defined in terms of variables. Changes can easily be made to the model by changing the values of the variables. In this manner it was easy to iterate the design and find the optimal geometry for our antenna. Within the HFSS interface the functions to create lines, rectangles, and circles are found under the Draw tab. The tools Boolean and Surface were used to add and subtract geometries and expand 2-dimensional shapes into 3-dimensions. Additionally, each object in the model is assigned a material. The materials used are shown in Table 3.1. Notice that the first five are conducting and the last three are dielectric materials. The Dupont and Rogers materials had to be defined manually through referencing manufacturer datasheets.

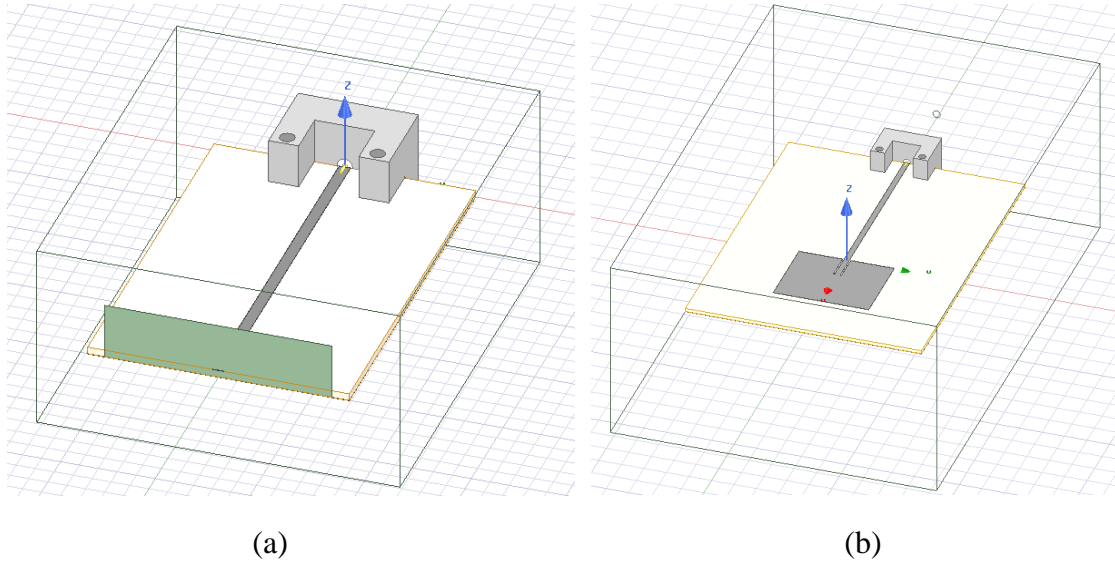
Table 3.1: Properties of conductor and dielectric materials used in the 3D model.

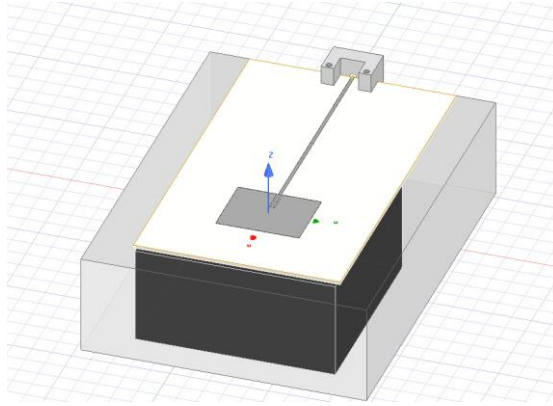
Name	Relative Permittivity	Relative Permeability	Bulk Conductivity (Ω^{-1}/m)	Dielectric Loss Tangent
Copper	1	0.999991	58000000	0
Gold	1	0.99996	41000000	0
Aluminum	1	1.000021	38000000	0
Nickel	1	600	14500000	0
Dupont KA801	1	1	1100000	0
Air	1	1	0	0
Teflon	2.1	1	0	0.001
Rogers RO3003	3	1	0	0.0013

The final step in creating our model was to assign boundary conditions and excitations. A radiation boundary was added to the surface of the airbox surrounding the antenna and to allow for waves to radiate infinitely far into space. The rule

requiring the airbox to be at least one quarter-wavelength from the radiating structure was followed [37]. By Equation (1-15) this is 15mm at a frequency of 5 GHz. Energy enters the antenna by means of a Southwest connector. To model this, a Wave Port excitation was defined. The characteristic impedance was set to $50\ \Omega$ and an integration line was drawn from the ground of the connector to the gold signal pin.

The three models that were constructed are shown in Figure 3.9. The first shows a Southwest connector and a microstrip transmission line that is fed into a rectangular waveport. This model was used to match the $50\ \Omega$ connector to the transmission line in order to ensure that there are minimal reflections at the feed point. The second model, Figure 3.9 (b), is an extension of the first and includes the antenna. There is a potential for reflections at the interface between the transmission line and the antenna and this was minimized through proper selection of the inset length as discussed in the previous section. Lastly, we modeled the antenna in the print environment to verify there are no significant effects on antenna performance.



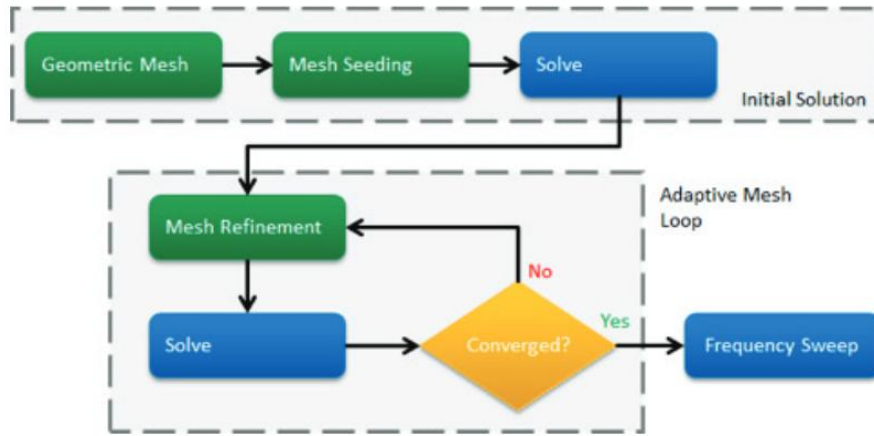


(c)

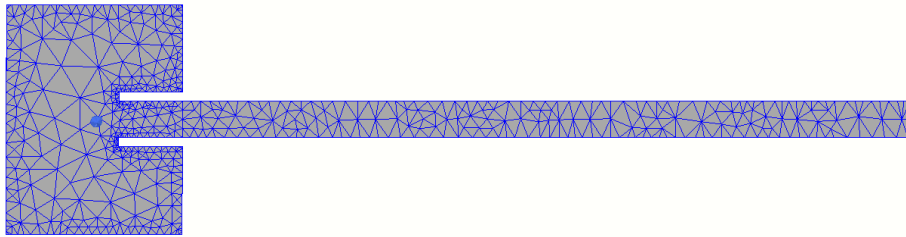
Figure 3.9: The three models developed in HFSS while designing the antenna.

3.4.2 Simulation Results

After constructing a model, simulations were run to investigate its behavior over a range of frequencies. HFSS is a FEM solver and works by dividing the model into discrete tetrahedral regions. This procedure is often referred to as “meshing.” The size of these regions is dependent on the frequency of interest and the required accuracy of the results. A high frequency will require smaller regions as will greater accuracy. Smaller meshes result in a greater simulation time and thus a balance needs to be achieved. HFSS is a particularly valuable tool because of the way in which it automatically generates and refines the mesh to generate accurate results and satisfy Maxwell’s equations throughout the entire model.



(a)



(b)

Figure 3.10: HFSS automatic adaptive meshing [38].

The reader interested in more detail on HFSS and FEM is referred to [38]. The meshing mechanism used by HFSS is outlined in Figure 3.10 (a). Figure 3.10 (b) shows the resulting mesh generated for our microstrip antenna. Notice that the mesh is finer in some areas such as by the edges. This allows localized electromagnetic behavior to be accounted for and guarantees accurate results.

Under the project manager pane, we select analysis and set up a driven solution with center frequency of 5 GHz. The minimum Delta S is left as 0.02 and the maximum number of passes is set to 12. A linear sweep including 801 points is defined from 3-7 GHz. Simulations were run locally and lasted on the order of 5-10

minutes per solution. Parametric sweeps were then defined for several of the important variables. The details and important conclusions will now be presented.

In the first model sweeps on the trace width were run. The width was selected because it is strongly correlated with the impedance for a microstrip line. A value of 1.2mm was finally settled upon. This width allows for upwards of 95% of the power to be transmitted to the second port. In the second model parametric sweeps were run for the length, width, inset length, and inset width. In analyzing the results, we relied heavily on a plot of the S11 parameter versus frequency. Our design goals were to obtain a resonant minimum of 5 GHz and for the magnitude of S11 to be below -15 dB at this frequency. This implies that only around 3% of the power is reflected. It was also important to see the ways in which the antenna performance might be affected by variations in other parameters and even several parameters simultaneously. It was apparent that the inset width was the most sensitive parameter in this regard.

In the second model we initially ran a simulation using the quantities calculated using the analytic approach of Section 3.3. A plot of S11 versus frequency shows the antenna performs reasonably well but can be improved. The resonant minimum was slightly less than what is desired and there are still some reflections present. To see this last point most vividly the complex reflection coefficient is shown on the smith chart below for 6.2mm as the blue line. The center of the smith chart represents the point where no power is reflected by the load impedance.

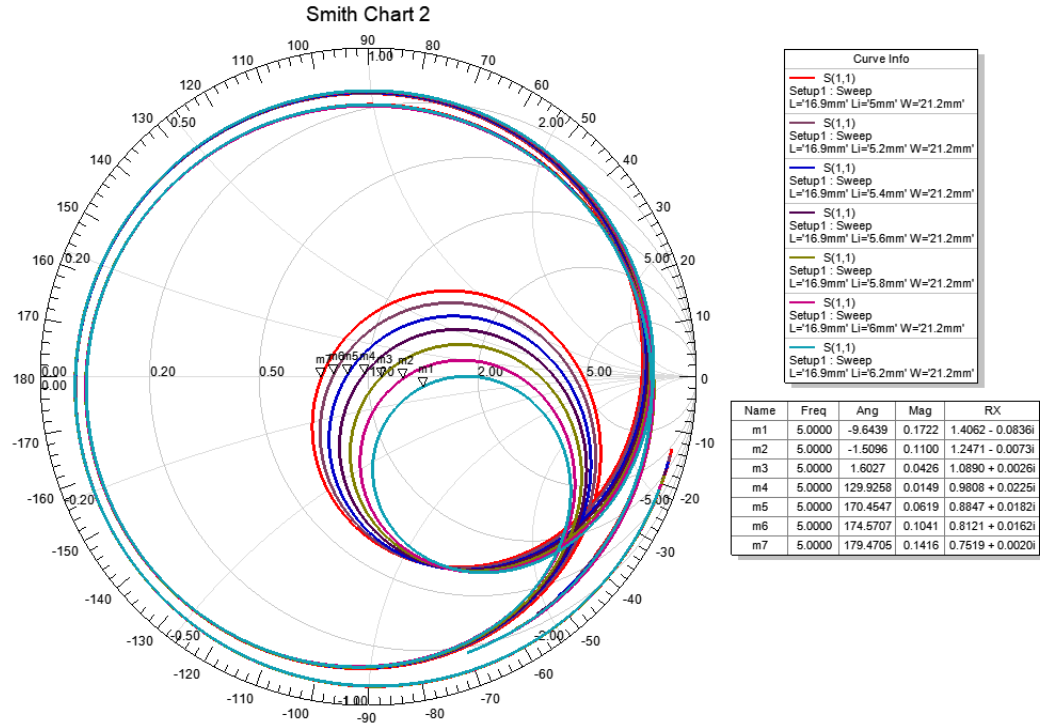
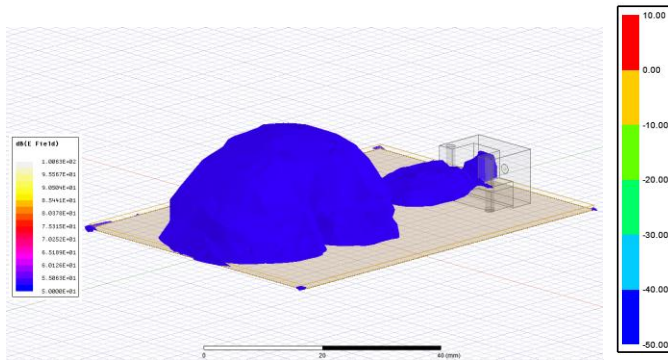


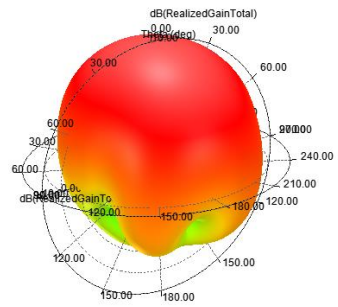
Figure 3.11: Smith chart showing sweep over inset length with length and width held constant. Markers show the 5 GHz points on each curve.

The goal is to optimize the parameters until the 5 GHz frequency point is at the center of the smith chart. The rest of the curves show 0.2 mm decrements in the inset length. The smith chart reveals that an inset length of 5.6 mm yields the smallest reflection coefficient and thus provides the best match for a frequency of 5 GHz.

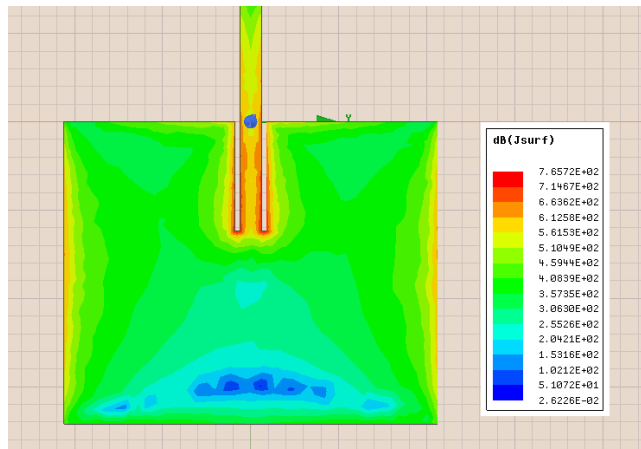
Plots of the magnitude of the electric field and magnitude of the surface current allowed us to check for any irregularities and gain greater intuition into the operation of the antenna. These are shown in Figure 3.12.



(a) Electric Field



(b) Absolute Gain



(c) Surface Current

Figure 3.12: Visualizing fields in HFSS to verify antenna performance.

Figure 3.12 (a) shows the propagation of the electric field in the microstrip transmission line is a quasi-TEM wave as expected. The absolute gain, discussed in Section 1.9.4, is plotted in Figure 3.12 (b) for a 3D spherical coordinate system and shows a peak of about 10 dB. Figure 3.12 (c) shows the magnitude of the surface current on the antenna. From an animation showing the time-evolution of the current the patch antenna we were able to verify that the antenna is single mode.

Table 3.2: Comparison of the results from the analytical and numerical analysis. Notice that all units are given in mm.

	Analytical	Numerical
Length of patch, L	17.1	16.9
Width of patch, W	21.2	21.2
Thickness of patch, t	0.03	0.03
Length of inset, y_0	6.2	5.6
Width of inset, W_i	0.3	0.3
Width of feed, W_0	1.2	1.2

Chapter 4

IMPLEMENTING THE CONTROL PROCESS

4.1 Overview

The previous two chapters were concerned with the theoretical aspects of introducing feedback control in AM and designing a patch antenna. This section will explain the practical details, including a manual for the interface we developed to control the CLAM process and a summary of our results.

The setup used to integrate the measurement apparatus into the AM process is shown in Figure 4.1. The plastic spacing element and aluminum heating block are necessary to isolate the connector and coaxial cable that connect to the VNA, from the printer's heated build plate. The aluminum block has the sole purpose of sourcing heat from the build plate to the portion of the substrate where micro-dispensing occurs. Since it is below the ground plane of the antenna it should have negligible effect on the S-parameters measured during the print.

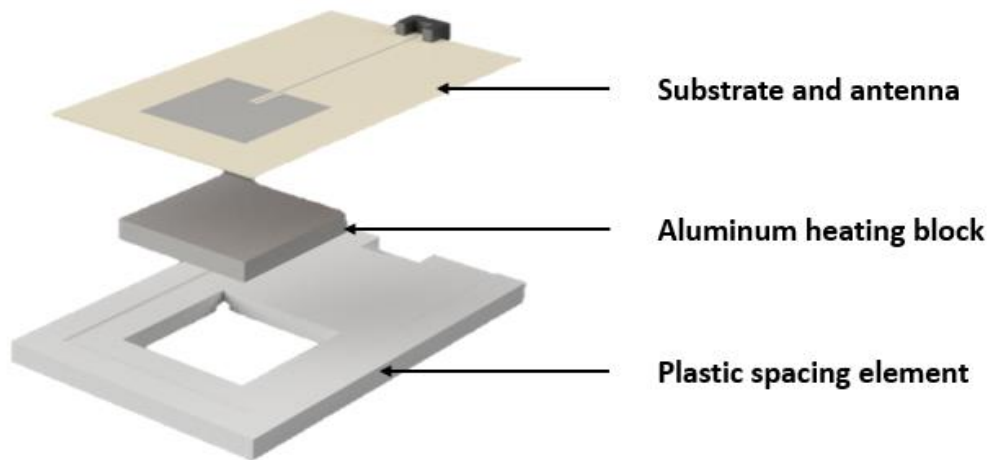


Figure 4.1: Setup devised to allow in-situ measurements to be taken. Created using Autodesk™ Fusion 360.

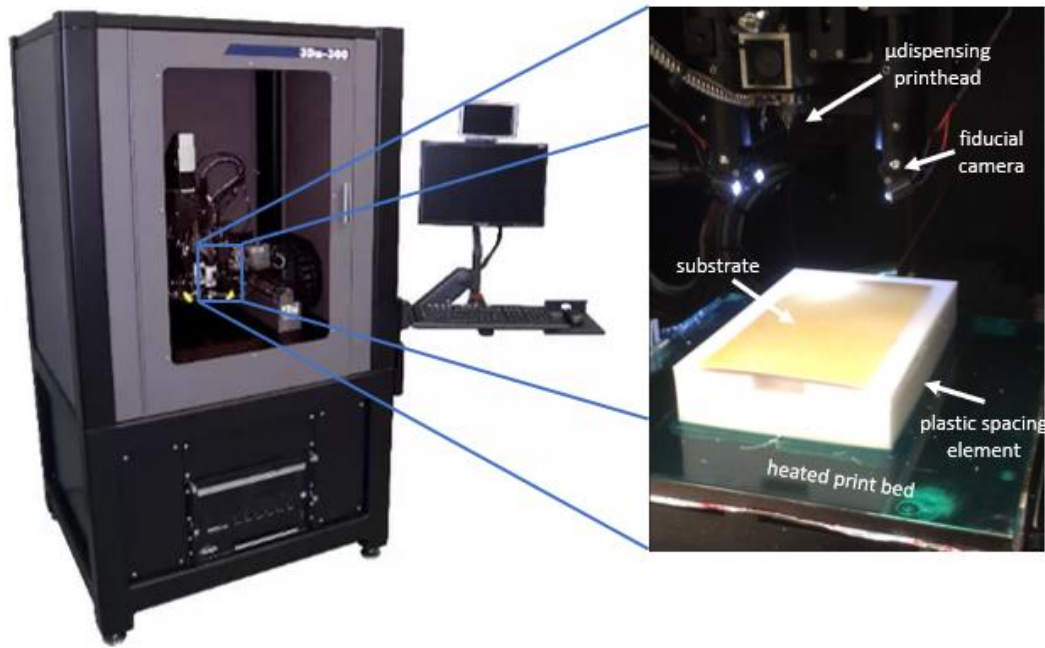


Figure 4.2: nScript 3Dn-300 system used for fabricating the patch antenna [39]

Fabrication was done using an nScript 3Dn-300 system which is shown in Figure 4.2. The nScript 3Dn-300 has various fabrication methods including fused deposition modeling (FDM), paste extrusion, pick-and-place, and milling. In our work only the paste extrusion capability was utilized. Linear brushless servomotors provide a maximum speed of 500 mm/s. The build area is 300x300 mm and x/y resolution spans from 10nm – 1 μ m. [39]. The nScript SmartPump™ is able to deposit materials with viscosities ranging from about 1 – 10⁶ cP. Perhaps the most important metric for our purposes was the minimum achievable line width that can be printed using the Dupont KA801 material. This was found to be approximately 100 μ m or 0.1 mm. See Section 2.3.1 for an in depth discussion on how the minimum line width of the printer is relates to the accuracy that can be achieved using the CLAM process.

4.2 Preparing the Substrate

The substrate used is Rogers Board R03003 with a thickness of 0.76mm (see Section 3.3). Before printing the copper plane on one side of the Rogers Board must be removed. The side containing the ground plane was covered with a coat of black paint. To the side with copper exposed, a solution containing Iron(III) Chloride (FeCl_3) was applied. Figure 4.3 (a) shows the exposed substrate after copper has been removed. The protective paint covering is then removed using a solution containing acetone. This beginning of this is shown in Figure 4.3 (b).



Figure 4.3: Process used to prepare the substrate. (a) shows the exposed substrate after etching and (b) shows the protective paint layer covering the ground plane being removed in the demasking process.

4.3 Control Interface Manual

The closed-loop manufacturing process discussed in Chapter 2 is implemented in MATLAB. The custom user interface is designed to be flexible and easily adapted for a variety of practical manufacturing scenarios. Information gleaned from the

program is constantly presented to the user in the form of graphs and messages displayed in the text pane.

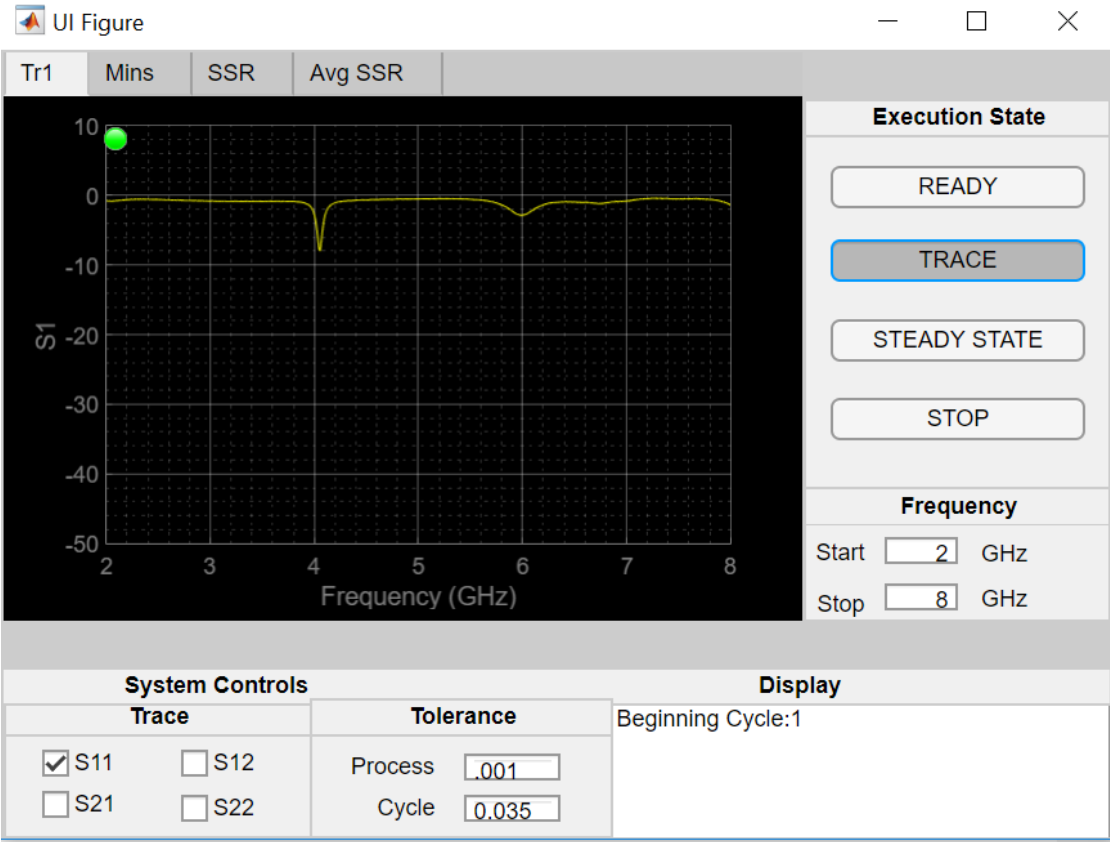


Figure 4.4: MATLAB control interface

Keysight Command Expert was used to find the commands needed to connect to and control the network analyzer. These were translated to MATLAB which works through calls to the Instrument Control Toolbox. When the interface is first opened the control light will appear red and a pop-up text box will prompt the user to calibrate the network analyzer. After the user has finished calibrating the user should click the box that says “ok.” The text display pane in the bottom right of the interface will display

details about the connection including the instruments identifying number. The control light will now appear yellow to indicate that the interface is in the ready state and can at any time begin recording data. This can be done by clicking “trace.” Upon entering the trace state, the light will turn green and the S-parameter will be displayed.

The system enters steady state when it detects a change between successive measurements that is below the cycle threshold as described by Equation (2-8). When steady state is reached a pop-up display asks the user to confirm that steady state has indeed been reached. The user should reference the tabs SSR and Avg SSR which display the values of Equations (2-7) and (2-8) as they evolve in time. To begin the next cycle the user clicks trace again.

The Mins tab is updated after every cycle and shows the error as defined in Equation (2-1). When the error is below the process threshold as described in Equation (2-2) the print is completed. When the user verifies this the control light turns red and the stop state has been reached. Pseudocode summarizing the interface is given below.

```
algorithm CLAM interface is
  get user input
  produce nearly the target value of the part
  establish connection to network analyzer
  if state is trace then
    while error greater than process threshold do
      increment antenna length
      while not in steady state do
        measure S-parameter
        check if reached steady state
      end
      record minimum and determine error
      display graphs
      wait for user to verify next cycle
    end
  end
  save data and end connection to network analyzer
end
```

Trace	
<input checked="" type="checkbox"/> S11	<input type="checkbox"/> S12
<input type="checkbox"/> S21	<input type="checkbox"/> S22

Figure 4.5: Pane showing which S-parameter is measured and plotted.

The trace pane has check boxes that allows the user to select which S-parameter is read from the network analyzer and plotted. During the closed-loop manufacturing process S11 should be selected and upon starting the program this is the default. There are situations prior to starting the process in which it might be useful to see other S-parameters and the user is therefore given that flexibility.

Tolerance	
Process	<input type="text" value=".001"/>
Cycle	<input type="text" value="0.035"/>

Figure 4.6: Pane where user can set process and cycle tolerance parameters.

The tolerance pane holds the values of the process and cycle tolerance parameters. The cycle parameter is a threshold value which if the program passes below for a given time causes the program to enter the steady state condition. The process parameter is likewise a threshold value but dictates when the entire manufacturing process ought to be concluded. The process is over when the resonant minimum is within the process parameter value of the desired resonant minimum or has exceeded the desired resonant minimum.

Frequency		
Start	<input type="text" value="2"/>	GHz
Stop	<input type="text" value="8"/>	GHz

Figure 4.7: Pane showing the frequency range over which measurements are taken.

The frequency pane allows the user to specify the start and stop frequencies. The network analyzer then records the S-parameter at 801 points spaced evenly over this frequency interval.

Chapter 5

CONCLUSION AND FUTURE WORK

5.1 Conclusion

This work has demonstrated some advantages of introducing feedback-control when fabricating antennas that have strict performance specifications using AM. The production cycle traditionally separates fabrication from testing and quality assurance. CLAM integrates these together reducing waste, improving throughput, and guaranteeing more accurate parts.

In Chapter 2 the details of the CLAM process were discussed for the general case and then for the specific case of fabricating antennas. The limitations of this process were clearly outlined. Measurements must be nondestructive and nondisruptive to the print process. Furthermore, to achieve accurate results the resolution of the printer must be such that sufficiently small gradations in the parameter of interest can be realized. Since micro-dispensing was used to conduct structures an additional step had to be added in which the steady state was detected before the final measurement was logged and the error calculated.

Since our purpose was to simply validate an idea, the error correction scheme used was quite primitive. An error of any amount above the process threshold directed the 3D printer to simply extend the length of the antenna by the smallest amount possible. A detailed account of how this corrects for errors was given in Chapter 3. It should be emphasized to the reader wishing to employ CLAM for a different purpose that significant time ought to be devoted early on in the design process to developing an appropriate model and understanding how the addition of material effects the property of interest.

5.2 Future Work

The work presented in this thesis is a synthesis of ideas coming from several disciplines and future work will involve advances in each of these areas. In the field of materials science work must be done to increase the palette of materials 3D printers can handle. Lowering the cost of printable conductors with low resistivity and dielectrics with low loss tangents is particularly important.

In the area of manufacturing advances to the core AM technologies are likely to continue and will make feedback control even more pertinent. The methods of nondestructive measurement were presented though only electromagnetic testing was used in our work. Future work is needed to integrate multiple measurement systems targeting different parameters into the same AM platform. Though the general CLAM process presented should hold across a wide array of practical use cases differences will exist. For example, in our case we had to ensure that steady state was reached before recording the resonant frequency. Software for creating models and controlling the manufacturing process are also needed.

Our work dealt strictly with employing feedback to increase the accuracy of the resonant frequency of an antenna. The information provided by a network analyzer can also be used to improve the efficiency of an antenna through minimizing reflection losses. Speaking practically, this might be done by, instead of incrementally increasing the length of the antenna, increasing the width of the antenna. Feedback control can be used for impedance matching in a wide variety of RF/microwave circuits. The appropriate addition of material behaves as a shunt or stub reactance that can be used for tuning. Developing the models and controllers needed to reach this goal is another area of exciting work to be done in the near future.

REFERENCES

- [1] A. Rida, L. Yang, R. Vyas and M. M. Tentzeris, "Conductive Inkjet-Printed Antennas on Flexible Low-Cost Paper-Based Substrates for RFID and WSN Applications," in *IEEE Antennas and Propagation Magazine*, vol. 51, no. 3, pp. 13-23, June 2009.
- [2] M. Ahmadloo and P. Mousavi, "A novel integrated dielectric-and-conductive ink 3D printing technique for fabrication of microwave devices," *2013 IEEE MTT-S International Microwave Symposium Digest (MTT)*, Seattle, WA, 2013, pp. 1-3.
- [3] P. Pa, Z. Larimore, P. Parsons and M. Mirotznik, "Multi-material additive manufacturing of embedded low-profile antennas," in *Electronics Letters*, vol. 51, no. 20, pp. 1561-1562, 1 10 2015.
- [4] T. P. Ketterl *et al.*, "A 2.45 GHz Phased Array Antenna Unit Cell Fabricated Using 3-D Multi-Layer Direct Digital Manufacturing," in *IEEE Transactions on Microwave Theory and Techniques*, vol. 63, no. 12, pp. 4382-4394, Dec. 2015.
- [5] C. M. Shemelya *et al.*, "3D printing multi-functionality: Embedded RF antennas and components," *2015 9th European Conference on Antennas and Propagation (EuCAP)*, Lisbon, 2015, pp. 1-5.
- [6] G. P. Le Sage, "3D Printed Waveguide Slot Array Antennas," in *IEEE Access*, vol. 4, pp. 1258-1265, 2016.
- [7] O. A. Peverini *et al.*, "Selective Laser Melting Manufacturing of Microwave Waveguide Devices," in *Proceedings of the IEEE*, vol. 105, no. 4, pp. 620-631, April 2017.
- [8] Z. Larimore, S. Jensen, A. Good, A. Lu, J. Suarez and M. Mirotznik, "Additive Manufacturing of Luneburg Lens Antennas Using Space-Filling Curves and Fused Filament Fabrication," in *IEEE Transactions on Antennas and Propagation*, vol. 66, no. 6, pp. 2818-2827, June 2018.
- [9] Jordan, John M. *3d Printing.*, 2018. Print.
- [10] Çakir, O.; Yardimeden, A.; Özben, T. (August 2007). "Chemical machining" (PDF). *Archives of Materials Science and Engineering*. 28 (8): 499–502.
- [11] A. Gomez-Torrent *et al.*, "A study of the additive manufacturing technology for RF/microwave components," *2017 11th European Conference on Antennas and Propagation (EUCAP)*, Paris, 2017, pp. 567-571.

- [12] R. X. Rodriguez, "Characterization of direct print additive manufacturing process for 3D build of a carbon nanostructure composite," Aug. 2014. Internet resource. http://emlab.utep.edu/pdfs/MSThesis_RicardoRodriguez_NPDF.pdf#page58
- [13] A. J. Good, "Additive manufacturing of passive beamforming systems," May 2019. Print
- [14] IEEE Standard for Definitions of Terms for Antennas," in *IEEE Std 145-2013 (Revision of IEEE Std 145-1993)* , vol., no., pp.1-50, 6 March 2014
- [15] Balanis, Constantine A. *Advanced Engineering Electromagnetics*. J. Wiley & Sons, 2012.
- [16] Balanis, Constantine A. *Antenna Theory: Analysis and Design*. J. Wiley & Sons, 2005.
- [17] Pozar, David M. *Microwave Engineering*. Hoboken, NJ :Wiley, 2012.
- [18] Radmanesh, Matthew M. *Radio Frequency and Microwave Electronics Illustrated*. Upper Saddle River, NJ: Prentice Hall, 2001. Print.
- [19] <https://www.keysight.com/en/pd-1349333-pn-E8361C/pna-microwave-network-analyzer?cc=US&lc=eng>
- [20] <https://www.fcc.gov/engineering-technology/policy-and-rules-division/general/radio-spectrum-allocation>
- [21] Phillips, Charles L, and John M. Parr. *Feedback Control Systems*. Boston: Prentice Hall, 2011. Print.
- [22] https://www.asnt.org/MajorSiteSections/NDT-Resource-Center/Codes_and_Standards/Codes_and_Standard_Bodies.aspx
- [23] K. Garanger, "Introducing the foundations of a general framework for closed-loop control in additive manufacturing via in situ measurements and semantic annotation," May 2018. Internet resource. <https://smartech.gatech.edu/bitstream/handle/1853/59957/GARANGER-THESIS-2018.pdf>
- [24] Pa, Peter. *Additive Manufacturing of Electromagnetic Multifunctional Composites.*, 2016. Internet resource.

http://udspace.udel.edu/bitstream/handle/19716/17602/2015_PaPeter_PhD.pdf?sequence=1&isAllowed=y

[25] Skolnik, Merrill I. *Introduction to Radar Systems*. Boston: McGraw Hill, 2001. Print.

[26] Bancroft, Randy. *Microstrip and Printed Antenna Design*. Raleigh, NC: SciTech Pub, 2009.

[27] James, James R, and P S. Hall. *Handbook of Microstrip Antennas*. London, U.K: P. Peregrinus on behalf of the Institution of Electrical Engineers, 1989.

[28] Lewin, L. "Radiation from discontinuities in stripline," *Proc. IEE*, 1960, 107C, pp. 163-170.

[29] R. Munson, "Conformal microstrip antennas and microstrip phased arrays," in *IEEE Transactions on Antennas and Propagation*, vol. 22, no. 1, pp. 74-78, January 1974.

[30] W. Gregorwich, "An electronically despun array flush-mounted on a cylindrical spacecraft," in *IEEE Transactions on Antennas and Propagation*, vol. 22, no. 1, pp. 71-74, January 1974.

[31] C. Peixeiro, "Microstrip patch antennas: An historical perspective of the development," *2011 SBMO/IEEE MTT-S International Microwave and Optoelectronics Conference (IMOC 2011)*, Natal, 2011, pp. 684-688.

[32] Lee, Kai F, and Wei Chen. *Advances in Microstrip and Printed Antennas*. New York: Wiley, 1997.

[33] R. F. Harrington, *Time-Harmonic Electromagnetic Waves*. New York: McGraw-Hill, 1961.

[34] Johnson, Richard C. *Antenna Engineering Handbook*. McGraw-Hill, 1993.

[35] E. O. Hammerstad, "Equations for Microstrip Circuit Design," *1975 5th European Microwave Conference*, Hamburg, Germany, 1975, pp. 268-272.

[36] A. Derneryd, "A theoretical investigation of the rectangular microstrip antenna element," in *IEEE Transactions on Antennas and Propagation*, vol. 26, no. 4, pp. 532-535, July 1978.

[37] <http://anlage.umd.edu/HFSSv10UserGuide.pdf>

[38] <https://www.ansys.com/-/media/ansys/corporate/resourcelibrary/application-brief/ab-ansys-hfss-adaptive-broadband-meshing.pdf>

[39] nScript, Inc., nScript, Inc., 2015. [Online]. Available: nscript.com. [Accessed 2019]